Author response to comments on «57 years (1960–2017) of snow and meteorological observations from a mid-altitude mountain site (Col de Porte, France, 1325 m alt.)» by Yves Lejeune et al.

The authors are grateful to the 3 referees for the time they devoted to review the manuscript and for their useful comments. Below is a point by point response to each comments. Authors responses are in blue and changes in the manuscript are enlightened in **bold**.

Comment by R. L. H. Essery (Referee #1)

Additional changes in the manuscript :
The dataset of snow vertical profiles has been extended to March 2018 (April 2015 in the first version of the manuscript) and these profiles are now provided in caaml v6 format (caaml v5 in the first version).

The availability of such a long, comprehensive, well-maintained and well-documented dataset is important for snow modelling, and I am keen to see this paper published. I have only a few questions:

The authors are very grateful to R. Essery for his positive, careful and useful review of the manuscript. Below is a point by point response to each comments. Authors responses are in blue and changes in the manuscript are enlightened in **bold**.

page 2, line 14
It might be appropriate here to mention the important contribution of Col de Porte data to SnowMIP (doi:10.3189/172756404781814825) and ESM-SnowMIP (https://doi.org/10.5194/gmd-2018-153).

Thanks for the references that have been added in the manuscript which now reads : « ... (ONERC). **The CDP dataset has been used as driving and evaluation data in several snow model intercomparison projects : SnowMIP (Etchevers et al., 2004) and ESM-SnowMIP (Krinner et al., 2018).** »
The explicit reference to ESM-SnowMIP page 22 line 7 has been consequently removed.

page 2, line 20
The underlined text only covers instrument types and periods in tables. I do not think that the underlining is necessary.
The « track changes » with respect to the former description of the dataset (Morin et al., 2012) was requested so that the paper was referenced in the Living data process of ESSD. Since the two referees found it unnecessary and misleading, the underlining has been removed in the revised manuscript.

Section 2.1
It would be interesting to know a bit more about how the elevations and p_occ are measured.

The 1998 masks were measured using a theodolite and the 2018 ones using a compass and a clinometer. Values of p_occ were visually estimated. This information have been added in the text as follows :

“Table \ref{tab:driving}) with 5° resolution in azimuth for two dates: July 1998 (**using a theodolite**) and June 2018 (**using a compass and a clinometer**). Masks are provided as a .csv file (\href{http://dx.doi.org/10.17178/CRYOBSCLIM.CDP.2018.SolarMask}{doi:10.17187/CRYOBSCLIM.CDP.2018.SolarMask}), they contain 3 values for each azimuth that correspond to: lower elevation, upper elevation and occultation percentage (p_{occ}, **visually estimated**) defined as follows (Fig. \ref{fig:mask}).”

Figure 2 Some symbol indicating the direction of view would be preferable to the emoticons for camera locations.

The 3 cameras are hemispherical, this information was added in Figure 2 captions and the emoticons were replaced by dark blue asterisks. The caption now reads :

“Schematic view of the experimental sites with sensor locations. The sensors indicated in yellow are for meteorological variables. The sensors indicated in red are not used anymore as of 2018, and those in blue correspond to snow measurements. Areas 23 and 24 correspond to soil temperature and humidity measurements. The correspondance between numbering and sensors is indicated in Tables \ref{tab:driving}, \ref{tab:eval} and \ref{tab:quot}. **The three dark blue asterisks correspond to the three hemispherical** Webcam locations.”

New Figure 2 is shown below :

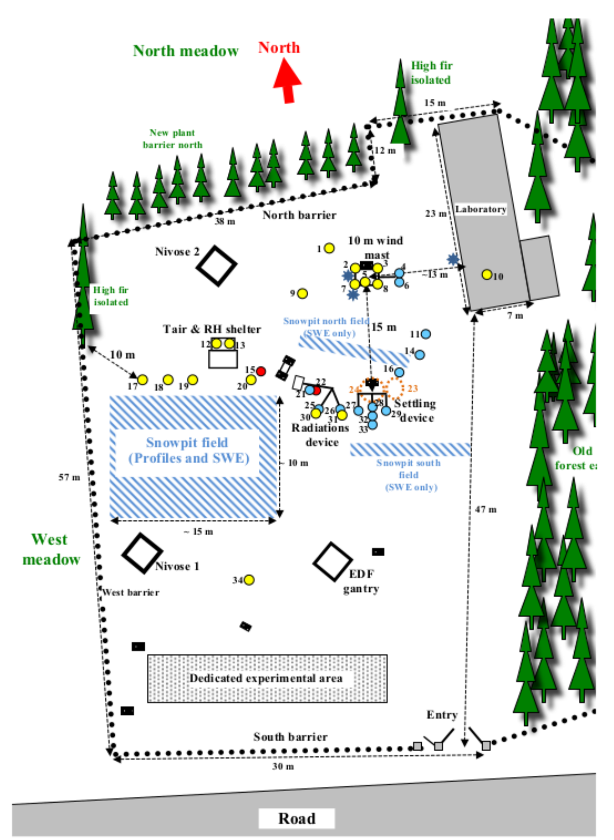

Figure 3 It is a little deceptive having the centre of the masks at 60 degrees elevation rather than

90 degrees.

Figure 3 has been modified, and the center of the mask is now 90° as shown below.

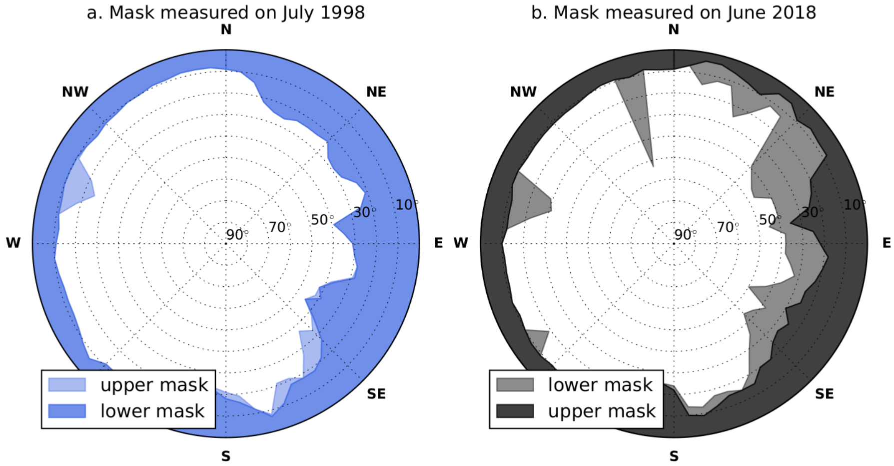

page 8, line 3 Is “available in that study” intended, i.e. Morin et al. (2012)?

Yes, we changed the sentence accordingly.

« The meteorological hourly dataset over 1993-2017 is an extension of the meteorological dataset provided in \citet{morin2012b} **in which an extensive description of the dataset is available.**»

page 8, line 23 Equation (2) will simplify a bit; is there a reason why this is not done? Does it always have one and only one solution for η in reasonable ranges of epsilon and e air ?

Thanks for this comment. There were several mistakes in Equations (1) and (2). The changes have been performed as follows :

“The first step of the procedure is to compute a cloudiness value, η (no unit, between 0 for clear sky and 1 for fully overcast) from measured air temperature T_{air} (K), longwave radiation LW_{down} (W m^{-2}) and specific humidity using Eqs. (\ref{eq:nebul1}) and (\ref{eq:nebul2}) from \citet{Berliand1952, **etchevers2000**}.

\begin{equation}
LW_{down}=**1.05** \varepsilon \sigma T_{air}^4
\label{eq:nebul1}
\end{equation}

\begin{equation}
\varepsilon=0.58+0.9k(\eta)+0.06\sqrt{e_{air}}(1-k(\eta))
\label{eq:nebul2}
\end{equation}

\begin{equation}
k(\eta)=(0.09+0.2\eta)\eta^2
\label{eq:nebul3}
\end{equation}

where σ is the Stefan-Boltzman constant, and e_{air} is the water vapour partial pressure calculated from measured T_{air} and relative humidity, expressed in hPa. **The correction factor 1.05 in Eq. (\ref{eq:nebul1}) accounts for the additional longwave radiation**

that is reaching the sensor due to the presence of surrounding trees. Eq. (\ref{eq:nebul2}) solution does not necessarily range between 0 and 1, η must be bounded between 0 and 1 when solving the equation."

page 9, line 7 The signs of the corrections are the wrong way round, aren't they?
Yes, thanks for noticing. This had been corrected.

Figure 6 The red temperature line is impossible to see on the red hardness bars.
Yes, the color of the temperature profile has been changed to black as shown below.

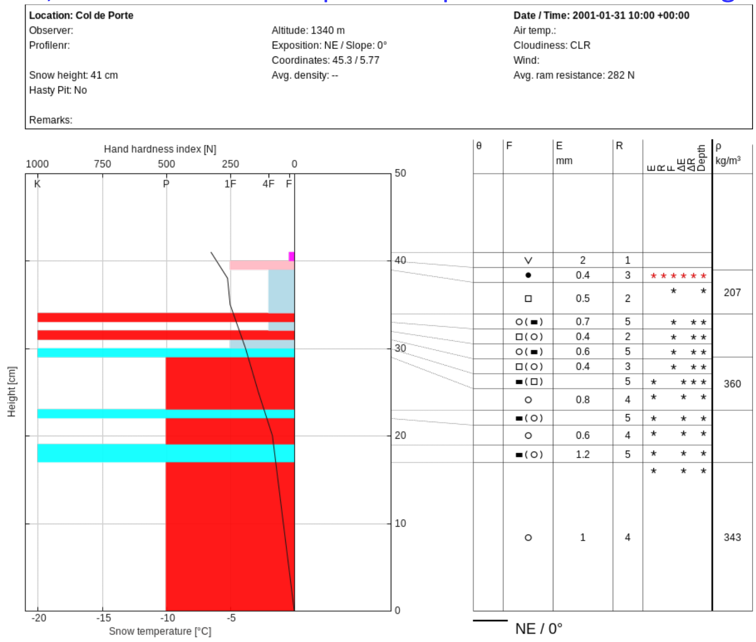

page 14, line6 I think that this means "mitigating the impact of undercatch", not the impact of the undercatch correction.
Yes, thanks for noticing. It has been corrected.

page 16, line 22 "mask measured in 2018"
Yes, thanks for noticing. It has been corrected.

page 16, line 26 The location of the total and diffuse radiation measurements is given as 2 here and 5 in the Figure 7 caption.
Thanks for noticing, the correct location is 5, it has been corrected in the text.

Figure 9 The (a) legend should be "Pit – reference"
Yes, this has been changed as shown below.

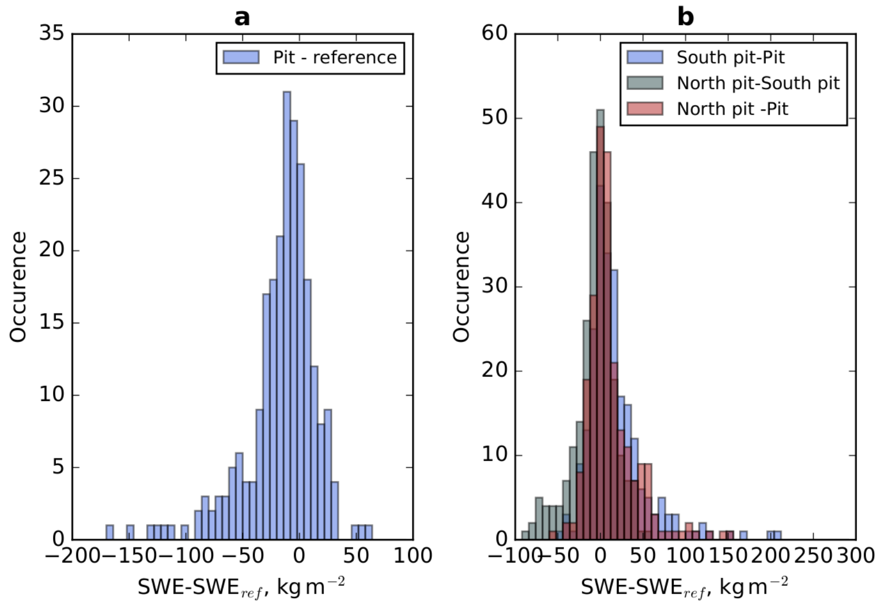

page 20, line 9 References to the first and second columns of Table 7 do not seem to make sense.

Yes. It has been modified. It is the first and second column of figure 10 not table 7. The sentences have been changed.

« The **left panels in Fig. \ref{fig:soil} display** the statistics of the different temperature probes at location 23 and spaced by roughly 10 cm. It indicates that the RMSD between the probes is lower than 0.25 K **(Tab. \ref{tab:soil})**. The **right panels in Fig. \ref{fig:soil} compare** locations 24 (old sensors) and 23 (new sensors) for two periods : summer (20 June to 10 October) and snow season (11 October to 19 June). During the snow season, the two locations show a small mean deviation of -0.11K and an RMSD of 0.42 K, while during summer the mean deviation is roughly -1.06 K leading to RMSD of 1.10 K **(Tab. \ref{tab:soil})**. Note that these two locations are spaced by only a few meters (see Fig. \ref{fig:scheme}). »

The writing is always clear, but I have sent the authors some minor corrections directly.

Thanks a lot for taking time to do the corrections, all corrections have been accounted for and are enlightened in the track-change pdf of the manuscript submitted along with the revised manuscript.

Comments by Anonymous Referee #2

Long term meteorological data are crucial for climate variability studies. It is of the utmost importance that these data are carefully collected, QCed, and stored, as well as fully documented (metadata). In that perspective, this paper presents a perfect example of the above, and it is important to support and promote such datasets to be available for the community.

The authors are very grateful to the anonymous reviewer for his/her positive, careful and useful review of the manuscript. A point by point response to each comment is provided in blue below. Changes in the manuscript are enlightened in **bold**.

Additional changes in the manuscript :
The dataset of snow vertical profiles has been extended to March 2018 (April 2015 in the first version of the manuscript) and these profiles are now provided in caaml v6 format (caaml v5 in the first version).

I recommend to accept this paper, with minor corrections, which are listed here:

- page 1, line 6: Unit is missing after 0.21.

It's ratio of irradiance so no unit. This has been added in the text.

- p1, l7: .... that can mainly be .... for snow water equivalent

Thanks, the sentence has been changed to :
« The estimated root mean squared deviation, **which mainly represents** spatial variability, is $\pm$ 10 cm for snow depth, $\pm$ 25 kg m^{-2} for snow water **equivalent** and $\pm$ 1 K for soil temperature ($\pm$ 0.4 K during the snow season). »

- p1, l9: Reduction of 39 cm in the mean snow depth, but what does it represent in %age of the mean total snow depth?

39 cm represents 40% of the mean total snow depth for the period 1960-1990. This information was added in the sentence as follow :
"The daily dataset can be used to quantify the effect of climate change at this site with a reduction of the mean snow depth (Dec. 1$^{\rm{st}}$ to April 30$^{\rm{th}}$) of 39 cm from 1960-1990 to 1990-2017 **(40 $\%$ of the mean snow depth for 1960-1990)** and an increase in temperature of + 0.90 K for the same periods."
This information has also been added page 22 line 6 :
"It demonstrates that the mean snow depth reduction between 1960-1990 and 1990-2017 is 39 cm (**40 $\%$ of the mean snow depth for 1960-1990**), while the air temperature has increased by 0.90 $^{\circ}$C over the same period and the total precipitation does not exhibit a significant trend."

- p1, l17: required to run and evaluate

The sentence has been changed accordingly.

- p2, l15: (i) to extend

Ok, this has been changed.

- p2, l16: (ii) to provide .... (iii) to provide
Ok, this has been changed.

- p2, l20: I do not understand this sentence, and could not find underlined text in the paper => remove (?)
The « track changes » with respect to the former description of the dataset (Morin et al., 2012) was requested so that the paper was referenced in the Living data process of ESSD. Since the two referees found it unnecessary and misleading, the underlining has been removed in the revised manuscript.

- p8, l7: Explain why the in-situ data are missing during Summer between 2011 and 2015
Historically, Col de Porte was dedicated to snow studies. Consequently, most of the sensors were removed and calibrated during summer. This is the reason why summer data are missing from 1993 to 2015 (see fig. 4 in Morin et al., 2014). In 2015, we decided to maintain the measurements during the whole year.
The text has consequently been modified as follows :
"The partitioning of the dataset between \textit{in-situ} data and the output of the meteorological analysis and downscaling tool SAFRAN \citep{durand1999, **durand2009**} is the same as in Fig. 4 of \citet{morin2012b}. For years 2011 to 2015, \textit{in-situ} data are restricted to the period 20 October of one year to 10 June of the next year. **Summer \textit{in situ} data are thus missing (calibration of the sensors during summer) from 1993 to 2015**. Starting on 10 June 2015, all data are \textit{in-situ} year-round except for very short periods with observation issues."

- p9, l5-10: The process of the correction is not "clear and clean" to me. Some information are missing: what is the Impact of a 10 W/m2 shift (or error) on the snowpack model? how does the final curve in Fig. 5 Looks like? is monthly average enough to assess the quality of the data (variation can be much higher on an hourly basis).

The impact of the longwave radiation correction on the simulations continuously increases along each winter season and becomes maximum during the melting period in spring. With the Crocus snowpack model, the yearly maximum difference in terms of snow depth ranges between 30 and 60 cm depending on the year, and between 150 and 300 kg/m² in terms of water equivalent of snow cover. In winter, a 2 K difference in surface temperature is common, with some much higher values. At the end of the season, the shift in the date of total melt out ranges between 5 and 10 days.

The curve in Fig. 5 corresponding to the final observation product is simply a plus or minus 10 W/m² shift during the two periods when the correction was considered necessary, as now shown by the green curve. This allows removing the breaks although there is still a noise between SAFRAN and observations. The bias identification was obtained from monthly comparisons between Col de Porte measurements and SAFRAN simulations for the Chartreuse massif at the same elevation. Only the significant temporal breaks in this difference can reasonably be attributed to instrumental issues. At shorter time steps (not shown here), and especially at an hourly time step, the differences between local observations and massif-scale simulations exhibit fluctuations, which are most likely due to local topographic effects, potential discrepancies between the local cloudiness and the simulated massif-scale cloudiness, etc. SAFRAN is the only other available reference because there was only one sensor. Therefore, it is unfortunately not possible to investigate with more temporal refinement the instrumental biases. Note also that the impact on snowpack simulations is mostly sensitive to systematic biases.

The text and figures were consequently modified as follows :

"Based on the hypothesis that the newest sensor **can be used as** a reference **because** it was fully calibrated at the **Physikalisch-Meteorologisches Observatorium (Davos, Switzerland)** outside and inside with a blackbody, the dataset was corrected as follow : -10 W m^{-2} from 1993 to November 2010 and +10 W m^{-2} from November 2010 to November 2015. **Since SAFRAN is the only available reference and does not account for local conditions, e.g. cloudiness, due to its coarse spatial resolution, it is unfortunately not possible currently to investigate with more temporal refinement this instrumental bias.** This correction, although **panning** the uncertainty values provided by the manufacturer, is of large significance for snowpack modelling considering the high sensitivity of the snowpack to **processes governed by** this variable (e.g. \citealp{raleigh2014, sauter2015, queno2017}). **Using the Crocus snowpack model with or without the corrections leads to a shift in the melt-out date ranging between 5 and 10 days (not shown).** "

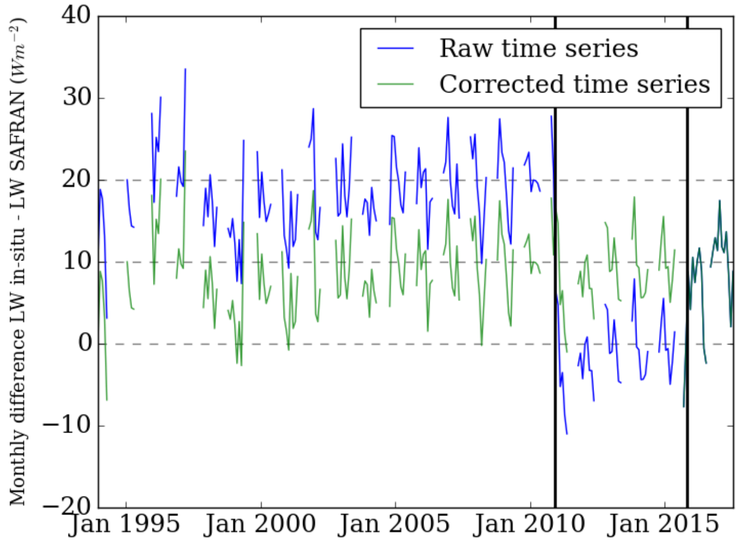

- Table 2: CGR4 (and not CRG4)

Thanks, it has been modified.

- p10, l3: What are the relevant sources of data (list)?

This information has been added in the text :

"Precipitation data are manually partitioned between liquid and solid phase using all relevant sources of data at the site, **namely snow depth, surface albedo, surface and air temperatures and differences between heated and non-heated rain gauges (locs. 1 and 9)**."

p10, l6-7: If wind data used to correct for undercatch is different, then the correction factors must also be different, right?

Yes, we agree and the sentence was misleading. Locations 15 (used before 2013) and 18 (used after 2013) are very close. Thus in this case, we believe it is reasonable to assume no difference in the correction factors.

The text has been updated as follows:

"From 2013 to 2017, the wind measurement used for the correction **was the one** placed at location 18 (Fig. \ref{fig:scheme}) **instead of location 15, since the ultrasonic sensor at location 18**

is more accurate than the wind sensor at location 15. Note that locations 15 and 18 are very close, i.e. a few meters, so that the wind speed values are not significantly different between the two locations. "

- p14, l4: .... not corrected for undercatch, in contrary ....
Ok, it has been corrected.

- p14, l5: .... by the same sensor used for rain and snow datasets
Ok, it has been corrected.

- p14, l6: Explain why the undercatch (and not the undercatch correction?) is mitigated when using the PG2000
The undercatch is inversely proportional to the collecting area. Since the PG2000 collecting area (2000 cm²) is 10 times larger than the GEONOR collecting area (200 cm²) , the undercatch is thus less important for the PG2000. The comparison in case of snowfalls between the PG2000 (not corrected for undercatch) and the GEONOR (corrected for undercatch) showed a very good agreement.
The information was added in the text as follows:
"The total precipitation dataset is measured with the PG2000 sensor, **for which the undercatch plays a minor role compared to the GEONOR due to the 10 times larger collecting surface area (Table 2)."**

- Table 5: For clarity, it should be moved in section 3.2 (where it is referenced)
Ok, Table 5 have been moved to section 3.2.

- p20, l13: Explain why the mean deviation is higher in summer (shading, surface properties?)
An explanation has been added in the paragraph as follows:
«The temperature difference between the two sensors may be attributed to differences in soil properties, local topography and shading. The larger differences in summer may be due to (i) larger heterogeneity in soil wetness and (ii) the absence of the snow cover that spatially tempers the surface temperature signal in winter.»

- I miss a short conclusion at the end of the paper. Few words summarizing the work
and the dataset available.
A short conclusion has been added to the paper and reads:
"**\conclusions**
This paper describes and provides access to the daily snow and meteorological dataset measured at the Col de Porte site, 1325 m a.s.l, Chartreuse, France for the period 1960-2017. The hourly dataset of snow and meteorological observations for the period 1993-2017 is made available along with weekly snow profiles from September 1993 to April 2015, soil properties and solar radiation masks. Based on measurements at several locations within the measurement field, we estimated the uncertainties and spatial variability of : the ratio between solar diffuse and total irradiance, snow depth, snow water equivalent and soil temperature. The data are placed on the repository of the Observatoire des Sciences de l\textquotesingle Univers de Grenoble (OSUG) datacenter :
\href{http://doi.osug.fr/public/CRYOBSCLIM_CDP/CRYOBSCLIM.CDP.2018.html}{http://dx.doi.org/10.17178/CRYOBSCLIM.CDP.2018}. "

Comments by C. Fierz

General comments

The authors present an important addition to the dataset described by Morin et al. in 2012. Not only is the hourly 2012 data set prolonged to 2017, but they also compiled all data available at Col de Porte in a daily dataset starting in 1960. The data are conveniently described and presented clearly and concisely without loosing on clarity, except for soil temperatures (see Section 3.4 in annotated manuscript). The estimation of uncertainties of the various measurements is an important asset of the paper as these are rarely given for other data sets. In conclusion, the paper is a welcomed contribution to long term, well described data sets for snow studies. Thus I recommend to accept the paper provided the authors address the points raised above and below as well as in the annotated version of their manuscript.

The authors are very grateful to Charles Fierz for his careful and useful review of the manuscript. A point by point response to each comment is provided in blue below. Changes in the manuscript are enlightened in **bold**.

Additional changes in the manuscript :

The dataset of snow vertical profiles has been extended to March 2018 (April 2015 in the first version of the manuscript) and these profiles are now provided in caaml v6 format (caaml v5 in the first version).

Specific comments

Regarding uncertainties on the water equivalent of snow cover (SWE), I have two questions:

1) Would it not be more interesting to compare the bulk density of the snow cover given by SWE/HS (where HS is snow depth) rather than SWE itself ? Indeed, I assume that the spatial variability of SWE is mostly given by the spatial variability of HS while measurement errors of the snow mass may dominate the uncertainty on bulk density. I am aware that the cosmic-ray sensor does not fully fit this approach, but I assume from Figure 2 that snow depth is quite well known at its location.

Yes, we agree that this would be interesting, especially regarding discussion on the spatial variability of the bulk density and its density such as in Sturm et al., 2010. Unfortunately, no snow depth sensor is located close enough to the reference SWE sensor (location 16 in Fig. 2). We are planning, in a near future, to add a snow depth sensor at this location. The snowpits data, which combine both SWE and HS measurements can be used to investigate the spatial variability of bulk density. Since the reference SWE sensor is not combined with snow depth measurement we believe that it is more relevant in that case to stick to the estimation of SWE variability and uncertainties.

Sturm, M., B. Taras, G.E. Liston, C. Derksen, T. Jonas, and J. Lea, 2010: Estimating Snow Water Equivalent Using Snow Depth Data and Climate Classes. *J. Hydrometeor., 11, 1380–1394,* https://doi.org/10.1175/2010JHM1202.1

2) If comparing SWE, I would prefer to see the differences expressed as a percentage of SWEref. But at least the mean maximum SWE should be indicated.

Translating Fig. 9 in percent of SWE ref would result in the following figure :

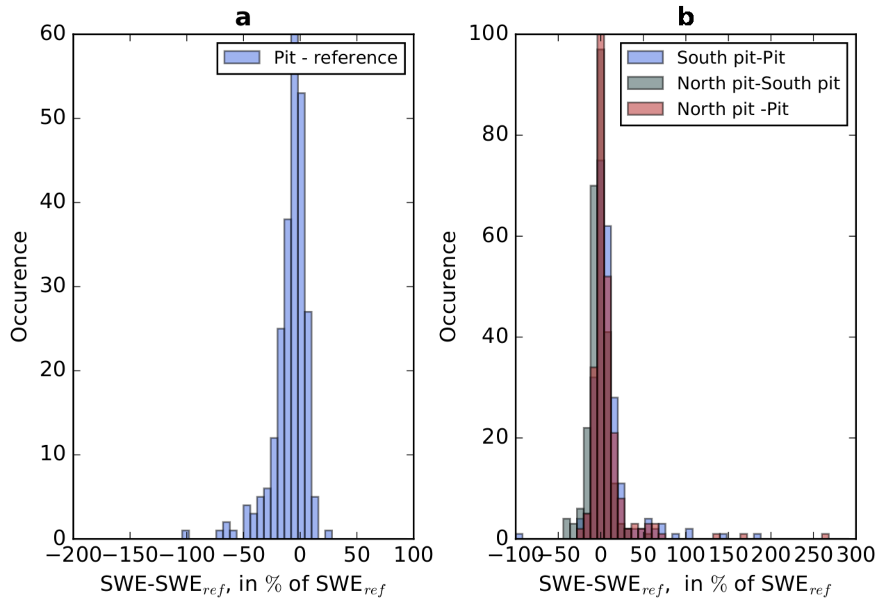

We believe that the representation with the absolute values give less emphasis on the outliers and thus we prefer to keep the analysis in absolute values in the revised manuscript. However, as suggested we added in the text the mean value of peak SWE and added the percentage in mean peak SWE in the description of the figure.

“Figure \ref{fig:swe} and Table \ref{tab:swe} compare the SWE automatic measurements at \hyperref[fig:scheme]{location 16} with the manual measurements from the main snow pit field (panel a) and the three locations for manual SWE measurements (panel b). The statistics are calculated over the 2001-2017 period. It must be underlined that the automatic SWE sensor is calibrated using the manual measurements at snow pit fields south and north. **The average of the annual maximum value of SWE$_{\rm{ref}}$ during this period is 389 $\pm$ 104 kg~m^{-2} .** Figure \ref{fig:swe} and Table \ref{tab:swe} show that the mean difference between the automatic and manual measurements in the main snow pit field reaches -17 kg\,m^{-2} with RMSD of almost 25 kg\,m^{-2}. The comparison between the three locations of manual measurements displays RMSD reaching 25 kg\,m^{-2}, **i.e. 8.6 $\%$ of average peak SWE values.** This value is consistent with the spatial variability of snow depth and can probably be used as an estimate of the uncertainty associated with the SWE dataset both due to measurement errors and spatial variability. “

Regarding Fig., Tab., etc, I would suggest to use the same style throughout the paper. Myself I would tend to use Figure, Table, Section, etc.

According to ESSD website (https://www.earth-system-science-data.net/for_authors/manuscript_preparation.html),

"The abbreviation "Fig." should be used when it appears in running text and should be followed by a number unless it comes at the beginning of a sentence, e.g.: "The results are depicted in Fig. 5. Figure 9 reveals that..."."

"Please note that the word "Table" is never abbreviated and should be capitalized when followed by a number (e.g. Table 4)."

"**Equations**: They should be referred to by the abbreviation "Eq." and the respective number in parentheses, e.g. "Eq. (14)". However, when the reference comes at the beginning of a sentence, the unabbreviated word "Equation" should be used, e.g.: "Equation (14) is very important for the results; however, Eq. (15) makes it clear that...""

"The abbreviation "Sect." should be used when it appears in running text and should be followed by a number unless it comes at the beginning of a sentence."

These guidelines have been taken into accounted in the new version of the manuscript (also pointed out by R. Essery). We also note that the Copernicus Editorial team will prepare the manuscript for final publication and enforce style issues that may have escaped our attention.

The reader often needs to navigate back to Figure 2 (and other Tables). I hope this can be made easier by linking any Location N to Figure 2 as well as referrals to tables to their respective Entries. That way the multiple repetition of '(Figure 2)' could be avoided in the text. Anyway, whatever you decide, make it consistent throughout the paper (currently not the case).

Tables references were already linked to their respective entries.

We have now linked every location to Figure 2 in .pdf.

This was also added in the legend of Figure 2 that now reads :

"...The correspondence between numbering and sensors is indicated in Tables \ref{tab:driving}, \ref{tab:eval} and \ref{tab:quot}. **For the sake of clarity, when a location is cited in the text, the reference to Fig. \ref{fig:scheme} is omitted and the location is directly linked to the figure or the corresponding table.** ..."

Moreover, I hope the final layout will also help with that respect. Currently, some Figures and Tables seem badly misplaced.

This formatting issue will be dealt with during the final editing process, upon acceptance of the manuscript, in connection with the publishing staff. The current locations of figures and tables have been also checked and updated (see also response to comment from referee #2).

Please also note the supplement to this comment: https://www.earth-syst-sci-data-discuss.net/essd-2018-84/essd-2018-84-RC3-supplement.pdf

Each comment and annotation in the supplement have been taken into account (please see the track-changes version of the manuscript submitted along with the revised version of the manuscript).

Regarding the comment of the HTN diff, the 80 cm difference values was a mistake in the dataset. Thanks for spotting it ! It has been corrected and Fig. 8 and the dataset has been updated consequently.

57 years (1960-2017) of snow and meteorological observations from a mid-altitude mountain site (Col de Porte, France, 1325 m alt.)

Yves Lejeune[1], Marie Dumont[1], Jean-Michel Panel[1], Matthieu Lafaysse[1], Philippe Lapalus[1], Erwan Le Gac[1], Bernard Lesaffre[1], and Samuel Morin[1]

[1]Univ. Grenoble Alpes, Université de Toulouse, Météo-France, CNRS, CNRM, Centre d'Etudes de la Neige, Grenoble, France

Abstract. In this paper, we introduce and provide access to ~~a~~ daily (1960-2017) and hourly (1993-2017) ~~dataset~~ datasets of snow and meteorological data measured at the Col de Porte site, 1325 m a.s.l, ~~Charteuse~~Chartreuse, France. Site metadata and ancillary measurements such as soil properties and masks of the incident solar radiation are also provided. Weekly snow profiles are made available from September 1993 to ~~April 2015.~~ March 2018. A detailed study of the uncertainties originating from both ~~measurements~~ measurement errors and spatial variability within the measurement site is provided for several variables. We show that the estimates of the ratio of diffuse to total shortwave broadband irradiance is affected by an uncertainty of ± 0.21 (no unit). The estimated root mean squared deviation, ~~that can be mainly attributed to~~ which mainly represents spatial variability, is ± 10 cm for snow depth, ± 25 kg m^{-2} for ~~snow water~~ water equivalent of snow cover and ± 1 K for soil temperature (± 0.4 K during the snow season). The daily dataset can be used to quantify the effect of climate change at this site with a ~~reduction~~ decrease of the mean snow depth (Dec. 1st to April 30th) of 39 cm from 1960-1990 to 1990-2017 (40 % of the mean snow depth for 1960-1990) and an increase in temperature of + 0.90 K for the same periods. Finally, we show that the daily and hourly datasets are useful and appropriate for driving and evaluating a snowpack model over such a long period. The data are placed on the repository of the Observatoire des Sciences de l'Univers de Grenoble (OSUG) datacenter : http://dx.doi.org/10.17178/CRYOBSCLIM.CDP.2018.

1 Introduction

The Col de Porte (CDP) site is a ~~meadow~~ mid-elevation meadow site located at 1325 m altitude (45.30° N, 5.77° E) in the Chartreuse moutain range. This observation site has been operated since 1959 in collaboration with several academic and non-academic partners (https://www.umr-cnrm.fr/spip.php?rubrique218). Daily measurements of snow depth, air temperature and precipitation amount have been performed since 1960. Hourly measurement of meterological and snow variables required ~~for running and evaluating~~ to run and evaluate detailed snowpack model such as Crocus (Brun et al., 1992; Vionnet et al., 2012) started in 1987 and have been almost continuous during the snow season since snow season 1993-1994. Measured data are manually and automatically checked and corrected using the measurements of several sensors and ~~if required~~ meteorological analyses (SAFRAN, Durand et al., 1999) if required, thus ensuring the quality and continuity of the dataset.

Such a dataset provides a unique framework to drive and evaluate snowpack models over a long period. Indeed Essery et al. (2013) demonstrated that the evaluation of snowpack models can be misleading if performed over only a few snow seasons~~only.~~

~~In the~~ . In recent years, such datasets with ~~a varying level of details~~ varying levels of detail have been made public for several snow sites (e.g. Essery et al., 2016) and have motivated the publication of a special issue in Earth System Science Data to gather openly available detailed meteorological and hydrological observational archives from long-term research catchments in well-instrumented mountain regions around the world. This initiative arises from a GEWEX Hydroclimatology Panel cross-cut project, INARCH, the International Network for Alpine Research Catchment Hydrology.

CDP is part of several ~~observations~~ observation networks at the local level (Observatoire des Sciences de l'Univers de Grenoble, OSUG), at the national scale (Observation pour l'Experimentation et la Recherche en Environnement CryObsClim and Systemes d'Observation et d'Experimentation au long terme pour la Recherche en Environnement des glaciers GlacioClim) and contributes to OZCAR (Observatoires de la Zone Critique Applications et Recherches), one of the French components of the eLTER European Research Infrastructure (International Long-term Ecological Research Networks, Gaillardet et al., in review). It is also ~~labeled as a member~~ a reference station of the World Meteorological Observation (WMO) Global Cryospheric Watch Cryonet network and of the INARCH network. CDP snow and meteorological observations have been selected as an indicator of climate change ~~effect~~ effects at medium elevation by the national climate change observatory (ONERC). ~~CDP~~ The CDP dataset has been used as driving and evaluation data in several snow model intercomparison projects : SnowMIP (Etchevers et al., 2004) and ESM-SnowMIP (Krinner et al., 2018). CDP is also an ideal place for specific snow related measurements campaigns, e.g. ~~intercomparison of measurement methods for solid precipitation~~ the WMO Solid Precipitation Intercomparison Experiment (SPICE), measurement of the spectral reflectance of snow (Dumont et al., 2017; Tuzet et al., 2017), snow surface roughness (Picard et al., 2016), snow under forest (Sicart et al., 2017).

The objectives of the present paper are (i) ~~extending~~ to extend the hourly dataset published in Morin et al. (2012) from 1993-2011 to 1993-2017, (ii) ~~providing~~ to provide a daily dataset over the 1960-2017 period and (iii) ~~providing~~ to provide estimates of the uncertainties of several variables due to both spatial variability within the observation site and measurements uncertainties. The paper first describes the site and the dataset. The second section is dedicated to ~~provide estimates of measurements~~ providing estimates of measurement uncertainties and spatial variability within the site and the last section describes some examples of the use of this dataset. ~~Text similar to Morin et al. (2012) is underlined.~~

2 Data description

The Col de Porte site (Fig. 1) is a grassy meadow surrounded by mainly coniferous (spruces) and some lobed-leave trees. All the instruments are located within an area of 40×50 m^2 (Fig. 2, ~~Tabs.~~ Tables 2, 3, 4). The height of the trees ranges from 10 to 40 m. Note that all datasets are provided in universal time coordinate (UTC).

~~Picture of the site taken on 2014-03-10 from the South barrier, looking toward North.~~

Figure 1. Picture of the site taken on 2014-03-10 from the South barrier, looking toward North.

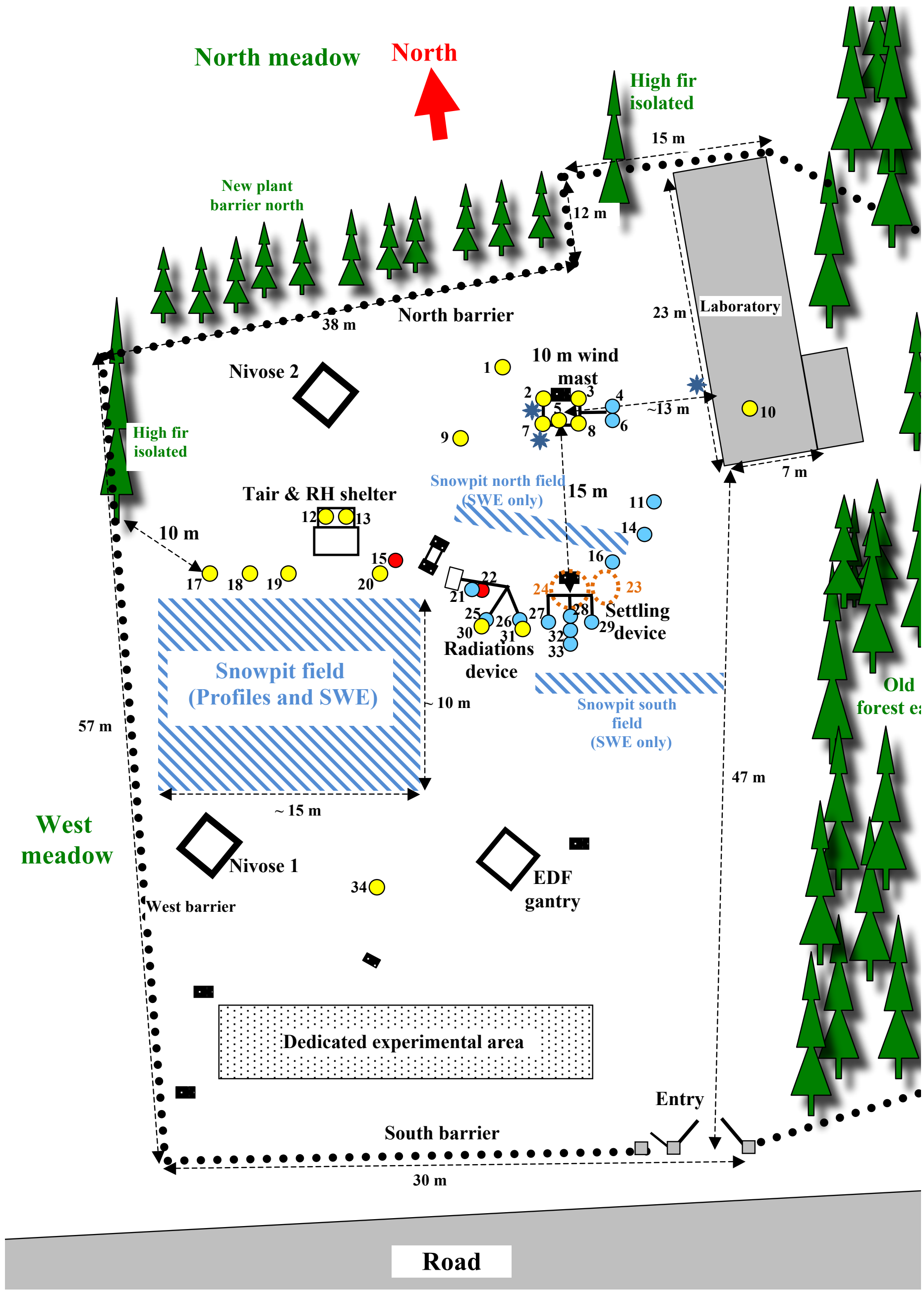

Figure 2. Schematic view of the experimental sites with sensor locations. The sensors indicated in yellow are for meteorological variables. The sensors indicated in red are not used anymore as of 2018, and those in blue correspond to snow measurements. Areas 23 and 24 correspond to soil temperature and humidity measurements. The correspondence between numbering and sensors is indicated in Tables 2, 3 and 4. For the sake of clarity, when a location is cited in the text, the reference to Fig. 2 is omitted and the location is directly linked to the figure or the corresponding table. The three dark blue asterisks correspond to the three hemispherical Webcam locations. The dedicated experimental area has been used for specific experiments, e.g. Dumont et al. (2017) or Bouilloud and Martin (2006).

~~Schematic view of the experimental sites with sensor locations. The sensors indicated in yellow are for meteorological variables. The sensors indicated in red are not used anymore as of 2018, those in blue corresponds to snow measurements. Areas 23 and 24 corresponds to soil temperature and humidity measurements. The correspondance between numbering and sensors are indicated in Tabs. 2, 3 and 4. The 3 emoticons correspond to the 3 Webcam locations.~~

2.1 Radiation masks

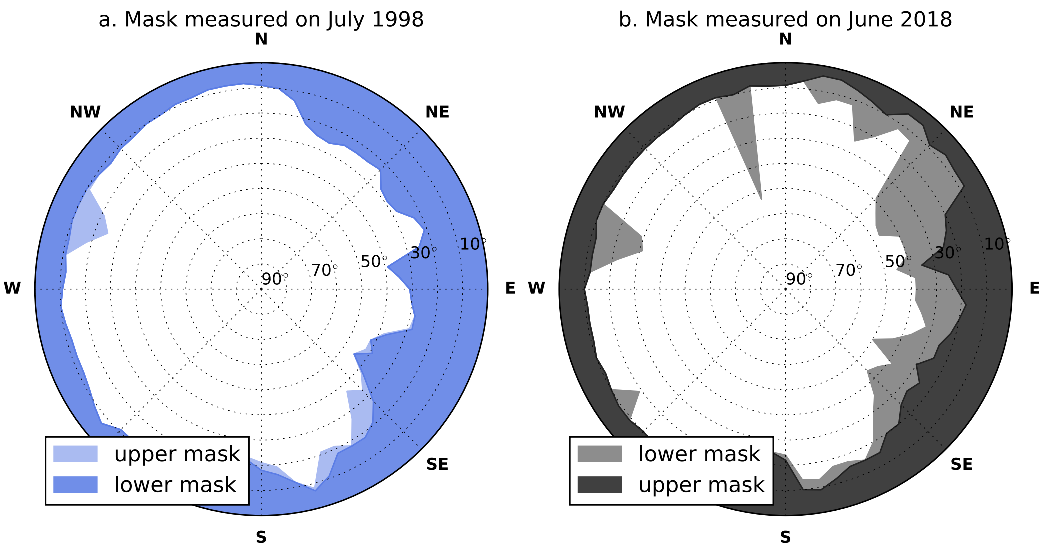

Figure 3. Masks measured at location 31 on July 1998 (left panel) and on June 2018 (right panel). Upper and lower mask elevations are represented by the coloured areas. Elevations are given in degrees, the center is 60 degrees elevation.

Surrounding trees and topography ~~are masking~~ mask part of the shortwave radiation. Masks were measured at ~~location 31~~ location 31 (corresponding to the measurements of the incoming shortwave radiation, see Fig. 2 and ~~Tab.~~ Table 2) with 5° resolution in azimuth for two dates: July 1998 ~~and June 2018.~~ (using a theodolite) and June 2018 (using a compass and a clinometer). Masks are provided as a .csv file (doi:10.17187/CRYOBSCLIM.CDP.2018.SolarMask), they contain 3 values for each azimuth that ~~corresponds~~ correspond to: lower elevation, upper elevation and occultation percentage (p_{occ}, visually estimated) defined as follows (Fig. 3). Below the lower mask elevation, there is no direct radiation. Above the upper mask elevation, 100 percent of the direct radiation is available and between the two, only $100 - p_{occ}$ percent of the direct radiation is available. These masks are applied for the calculation of the direct/diffuse shortwave incoming radiation as explained in ~~section~~ Sect. 2.3.1. The discrepancies between the two masks are most likely due to changes of the vegetation (growing and major ~~trees cut~~ tree cutting in 1999, see Morin et al., 2012).

~~Masks measured at location 31 on July 1998 (left panel) and on June 2018 (right panel). Upper and lower mask elevations are represented by the solid lines. Elevations are given in degrees, the center is 60 degrees elevation.~~

2.2 Soil and vegetation properties

Soil properties were measured close to ~~location 33 (see Fig 2)~~ location 33 on 29 September 2008, close to ~~location 24 on October 2nd~~ location 24 on 2 October 2012 and close to location 30 on 18 October 2017.

On 29 September 2008, the soil properties were measured over the first meter as illustrated by Fig. 4. The layering of the soil was estimated visually and is provided in ~~Tab.~~ Table 1. The soil properties (particles size analysis, organic matter, nitrogen and carbon total content) were also analyzed down to 87 cm depth. The dataset is provided as a .csv file (soil_properties_2008.csv). On ~~October 2nd~~ 2 October 2012, the same analysis was conducted over the first 30 cm of soil at ~~location 24~~ location 24 along with measurements of the soil dry density. The dataset is provided as a .csv file (soil_properties_2012.csv). The two .csv files are available as doi:10.17178/CRYOBSCLIM.CDP.2018.Soil.

Table 1. Visual characterization of the soil layers corresponding to Fig. 4 on 29 September 2008.

Top depth (cm)	Bottom depth (cm)	Visual texture
0	5	organic soil with grass roots
5	18	organic soil without roots
18	47	clay and sand
47	70	grey clay and sand
70	87	grey clay
87	100	pebbles and grey clay, no sampling

On 18 ~~october~~ October 2017, the soil densities were ~~analyzed~~ analysed for the first 30 cm. At that time, the soil dry density was 1100 $\pm$ 67 kg m^{-3} without considering the vegetation. The soil wet density was 1475 $\pm$ 59 kg m^{-3}. These values are the mean and standard deviation of 2 measurements over 0-10 cm depth and 2 at 20-30 cm depth close to ~~location 30.~~ location 30. No significant differences between the two sampling depths were ~~measured~~observed. On the same day, the vegetation (grass) dry and wet mass were measured on a 50 by 50 cm surface at the same location. The measurements result in a value of 1.92 kg m^{-2} for wet mass and 1.54 kg m^{-2} for dry mass. The height of the grass (roughly 5 cm) during the time of measurements can be considered as typical for late fall. Note that the grass is frequently cut during summer. These measured soil and vegetation properties can be useful ~~to constrain~~ for constraining soil and vegetation schemes which are often coupled with snowpack models (Decharme et al., 2013).

Figure 4. Soil profile of 1 meter depth performed close to ~~location 33~~ location 33 on 29 September 2008. The visual characterization provided in Table 1 can be seen on this picture.

2.3 Meteorological hourly data, 1993-2017

The meteorological hourly dataset over 1993-2017 is an extension of the meteorological dataset provided in Morin et al. (2012) ~~. An~~ in which an extensive description of the dataset is available~~in this study. Below are reported~~. Below only changes that happened after 2011 and additional details not provided in Morin et al. (2012) are reported.

The dataset is provided as a continuous hourly dataset since 1993, so that it can be easily used to drive snowpack models. The partitioning of the dataset between *in-situ* data and the output of the meteorological analysis and downscaling tool SAFRAN ~~(Durand et al., 1999)~~ (Durand et al., 1999, 2009b) is the same as in ~~figure~~ Fig. 4 of Morin et al. (2012). For years 2011 to 2015, *in-situ* data are restricted to the period ~~20th~~ 20 October of one year to ~~10th~~ 10 June of the next year. ~~Starting on 10th~~ Summer *in situ* data are thus missing (calibration of the sensors during summer) from 1993 to 2015. Starting on 10 June 2015, all data are *in-situ* year-round except for very short periods with observation issues. An *in situ* flag is provided together with the meteorological data (value = 1 for *in situ* data).

Table 2 provides an ~~udpate~~ update of the type of sensors used for meteorological measurements with respect to ~~Tab.~~ Table 1 in Morin et al. (2012). The dataset is provided in netCDF format (doi:10.17178/CRYOBSCLIM.CDP.2018.MetInsitu) in the standard format for SURFEX surface model meteorological inputs (Vionnet et al., 2012; Masson et al., 2013). The ~~atmopsheric~~ atmospheric pressure value corresponds to the mean climatological value at CDP.

2.3.1 Shortwave incoming radiation

The ~~meterological~~ meteorological dataset provides both total and diffuse incoming broadband ~~radiations at location 31.~~ radiation at location 31. The diffuse shortwave radiation is not measured but calculated from total shortwave and longwave incident radiation and air temperature as described in the following.

The first step of the procedure is to compute a cloudiness value, η (no unit, between 0 for clear sky and 1 for fully overcast) from measured air temperature T_{air} (K), longwave radiation LW_{down} (W m^{-2}) and specific humidity using ~~Equations 1and 2 from Berliand (1952)~~Eqs. (1) and (2) from Berliand (1952); Etchevers (2000).

$$LW_{down} = 1.05\varepsilon\sigma T_{air}^4 \tag{1}$$

$$\varepsilon = 0.58 + 0.9k(\cancel{0.09+0.2}\eta)\cancel{\eta^2} + 0.06\cancel{e_{air}-0.05*}\sqrt{e_{air}}(\cancel{1-}1-k(\cancel{0.09+0.2}\eta)\cancel{\eta^2}) \tag{2}$$

$$k(\eta) = (0.09+0.2\eta)\eta^2 \tag{3}$$

where σ is the Stefan-Boltzman constant, and e_{air} is the water vapour partial pressure calculated from measured T_{air} and relative humidity, expressed in hPa. The correction factor 1.05 in Eq. (1) accounts for the additional longwave radiation that

Table 2. Overview of the sensors used to gather the hourly meteorological data, between 1993 and 2017 at Col de Porte, France. The locations refer to Fig. 2.

Variable	Location	Sensor	Period of operation	Height	Unit	Integration method
Air temperature	12	PT 100/ 3 wires	... → 1996/1997	1.5 m*	K	Instantaneous
	12	PT 100/ 4 wires	1997/1998 → ...	1.5 m*	K	Instantaneous
	mast	PT 100/ 4 wires	1997/1998 → ...	3.1 m	K	Instantaneous
Relative humidity	13	SPSI MU-C.1/MUTA.2	... → 1994/1995	1.5 m*	%RH	Instantaneous
	13	Vaisala HMP 35DE	1995/1996 → 2005/2006	1.5 m*	%RH	Instantaneous
	13	Vaisala HMP 45D	2006/2007 → ...	1.5 m*	%RH	Instantaneous
Windspeed	2	Laumonier – heated	1997/1998 → ...	10 m	$\mathrm{m\,s^{-1}}$	Integrated (60 min)
	7	Chauvin Arnoux Tavid 87 – non-heated	whole record	10 m	$\mathrm{m\,s^{-1}}$	Integrated (60 min)
	15	Laumonier – heated	2000/2001 → 2014-2015	3.3 m	$\mathrm{m\,s^{-1}}$	Integrated (60 min)
	3	Thies Ultrasonic anemometer – heated	March 2012 → ...	10 m	$\mathrm{m\,s^{-1}}$	Integrated (60 min)
	18	Thies Ultrasonic anemometer – heated	Dec. 2013 → ...	3,3 m	$\mathrm{m\,s^{-1}}$	Integrated (60 min)
Inc. shortwave radiation	31	Kipp & Zonen CM7	... → 15 March 1996	1.2 m*	$\mathrm{W\,m^{-2}}$	Integrated (50 min)
	31	Kipp & Zonen CM14	15 March 1996 → Oct. 31st 2015	1.2 m*	$\mathrm{W\,m^{-2}}$	Integrated (50 min)
	31	Kipp & Zonen CMP10	Nov. 2015 → ...	1.2 m*	$\mathrm{W\,m^{-2}}$	Integrated (50 min)
Inc. longwave radiation	30	Eppley PIR	... → 2010/2011	1.2 m*	$\mathrm{W\,m^{-2}}$	Integrated (50 min)
	30	Kipp & Zonen CG4	2010/2011 → Oct. 2015	1.2 m*	$\mathrm{W\,m^{-2}}$	Integrated (50 min)
	30	Kipp & Zonen CGR4	Oct. 2015 → ...	1.2 m*	$\mathrm{W\,m^{-2}}$	Integrated (50 min)
Precipitation	9	PG2000 heated (2000 $\mathrm{cm^2}$), tipping bucket	whole record	2.75 m	$\mathrm{kg\,m^{-2}\,s^{-1}}$	Difference
	1	PG2000 non-heated (2000 $\mathrm{cm^2}$), tipping bucket	whole record	2.75 m	$\mathrm{kg\,m^{-2}\,s^{-1}}$	Difference
	20	GEONOR (200 $\mathrm{cm^2}$) with windshield, weighing gauge	whole record	3 m	$\mathrm{kg\,m^{-2}\,s^{-1}}$	Difference
	17◇	GEONOR T-200B-3 (200 $\mathrm{cm^2}$), weighing gauge	Dec. 2013 → ...	3.1 m	$\mathrm{kg\,m^{-2}\,s^{-1}}$	Difference
	19◇	GEONOR T-200B-3 (200 $\mathrm{cm^2}$) with windshield, weighing gauge	Dec. 2013 → ...	3.1 m	$\mathrm{kg\,m^{-2}\,s^{-1}}$	Difference
	34◇	OTT Pluvio 2 OTT (400 $\mathrm{cm^2}$) with windshield, weighing gauge	Dec. 2013 → ...	3.1 m	$\mathrm{kg\,m^{-2}\,s^{-1}}$	Difference⋆

* Height adjusted manually above snow surface (≈ weekly).

◇ The sensors were installed for the WMO SPICE project and are used in this study only to complement the dataset if a problem exists for the reference sensor.

⋆ Amount processed in non-real-time (filtered values).

is reaching the sensor due to the presence of surrounding trees. Eq. (2) solution does not necessarily range between 0 and 1, η must be bounded between 0 and 1 when solving the equation.

The calculated value of η is then used to partition the total measured shortwave radiation into direct and diffuse fraction using the radiative transfer model from Vauge (1983) and the measured mask described in ~~See~~Sect. 2.

An additional shortwave radiation sensor (Delta-T SPN1 -heated) ~~has been installed at location 5 (Fig. 2)~~ was installed at location 5 in September 2016 (9.5 m above ground) and measures both diffuse and total shortwave radiation over the 400-2700 nm range.

A comparison between these measured and calculated direct/diffuse ~~distribution~~ distributions is provided in ~~See~~Sect. 3.1.

2.3.2 Longwave incident radiation

The sensor for incident longwave radiation was replaced in October 2015 by a Kipp&Zonen CGR4 sensor (~~location 30 in Fig. 2~~location 30). Figure 5 displays the comparison of the measured incident longwave radiation with simulated longwave radiation from SAFRAN based on monthly ~~average~~averages. It shows that the ~~bias~~ deviation between SAFRAN and the measurements displays two large breaks ~~of 10 W m^{-2}~~ in October 2015 and in autumn 2010 (corresponding to another sensor replacement, ~~Tab.~~ Table 2). Based on the hypothesis that the newest sensor ~~is the reference since~~ can be used as a reference because it was fully calibrated ~~oustide~~ at the Physikalisch-Meteorologisches Observatorium (Davos, Switzerland) outside and inside with a blackbody, the dataset was corrected as follow : ~~+10~~ -10 W m^{-2} from 1993 to November 2010 and ~~-10~~ +10 W m^{-2} from November 2010 to November 2015. Since SAFRAN is the only available reference and does not account for local conditions, e.g. cloudiness, due to its coarse spatial resolution, it is unfortunately not possible currently to investigate with more temporal refinement this instrumental bias. This correction, although ~~ranging in~~ spanning the uncertainty values provided by ~~sensor manufacturor~~the manufacturer, is of large significance for snowpack modelling considering the high sensitivity of the snowpack to processes governed by this variable (e.g. Raleigh et al., 2015; Sauter and Obleitner, 2015; Quéno et al., 2017). Using the Crocus snowpack model with or without the corrections leads to a shift in the melt-out date ranging between 5 and 10 days.

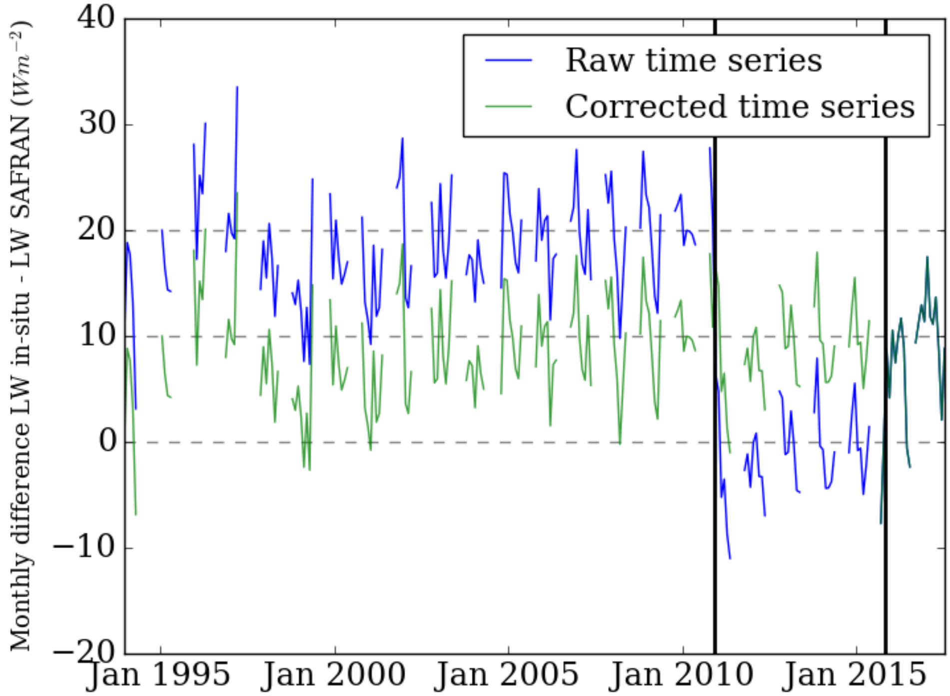

Figure 5. Monthly average of the difference between measured downward longwave and SAFRAN estimates. The two vertical black lines indicate the sensor changes (cf ~~Tab.~~ Table 2). The blue lines correspond to the raw time series and the green one to the corrected time series.

2.3.3 Precipitation

Precipitation data are handled according to Morin et al. (2012). Precipitation data are manually partitioned between liquid and solid phase using all relevant sources of data at the site, namely snow depth, surface albedo, surface and air temperatures and differences between heated and non-heated rain gauges (locations 1 and 9). The precipitation values provided in the dataset are based on the reference gauge, GEONOR, at ~~location 20.~~ location 20. Other OTT and GEONOR gauges are used ~~in complement to~~ to complement the reference sensor measurements. Hourly solid precipitation measurements are corrected for undercatch depending on temperature and wind speed, as described in Morin et al. (2012). From 2013 to 2017, the wind measurement used for the correction ~~is placed at location~~ was the one placed at location 18 instead of location 15, since the ultrasonic sensor at location 18 is more accurate than the wind sensor at location 15. Note that locations 15 and 18 ~~(Fig. 2), which better represents the wind at the level of the different precipitation gauges~~are very close, i.e. a few meters, so that the wind speed values are not significantly different between the two locations.

~~Overview of the sensors used to gather the hourly meteorological data, between 1993 and 2017 at Col de Porte, France. The index refers to the location of the sensor represented in Fig. 2.Text similar to Morin et al. (2012) is underlined.~~

2.4 Snow and soil data, 1993-2017

The ~~evaluation hourly~~ hourly evaluation dataset over 1993-2017 is an extension of the evaluation dataset provided in Morin et al. (2012). An extensive description of the dataset is available in the latter study. Below ~~are reported~~ only changes that happened after 2011 and additional details not provided in Morin et al. (2012) are reported. The hourly dataset is provided as a netCDF file (doi:10.17178/CRYOBSCLIM.CDP.2018.HourlySnow). Within this dataset, the soil temperature, soil humidity and settling disk temperature are raw measurements (uncorrected).

Table 3 provides an udpate of the type of sensors used for evaluation measurements with respect to ~~Tab.~~ Table 2 in Morin et al. (2012).

Starting ~~on~~ in October 2010, the snow depth at ~~location 32~~ location 32 has been measured with a Dimetix Laser ranger. The field-of-view is a few mm diameter spot and the accuracy provided by the manufacturer is ± 1.5 mm. Since October 2010, the snow depth ~~measurements~~ measurement provided in the dataset (reference snow depth) is the ~~measurements~~ measurement of the Dimetix Laser ranger. Data from the other ~~sensors~~ snow depth sensors and precipitation amount are used to ~~evaluate and~~ correct the Laser data from small artefacts.

The surface temperature reference values contained in the dataset mainly originates from the Kipp&Zonen ~~updward pyrgeometer (location 25~~upward pyrgeometer (location 25), same sensor as ~~location 30 in Tab.~~ location 30 in Table 2). Since september 2010, these data are complemented by the other surface temperature sensors with a conical field of view shown in ~~Tab.~~ Table 3. The reference surface temperature is bounded to 273.15 K when snow is present on the ground.

New sensors for soil temperature and humidity have been installed in October 2012 at several depths (-0.05, -0.1, -0.2, -0.3 m) at ~~location 23~~ location 23 close (roughly 2 m) to ~~location 24 (Fig. 2)~~ location 24 where the older soil temperature sensors were located. In total, for location 23, 3 probes are placed at 10 cm depth roughly 10 cm away from each other. In the following they are referred as s1_loc23_10, s2_loc23_10 and s3_loc23_10. At 20 cm depth, there is only two probes roughly 10 cm away from each other that are referred as s1_loc23_20, s2_loc23_20.

The differences between the measurements at these two locations are discussed in ~~See~~Sect. 3.4. It must be underlined that the soil humidity measurements show that the soil is almost always saturated by liquid water when snow is present. This characteristic may not be typical for mountain slopes (e.g. Williams et al., 2009) and may be difficult to reproduce with usual soil models.

The measurements of the vertical profile of snowpack properties as described in Fierz et al. (2009) are also provided in caaml format (version ~~5~~6) according to the International Association for Cryospheric Science (IACS) standard. They can be visualized using the niViz software ~~.~~ (niviz.org). An example is displayed in Fig. 6 for 13 January 2001. These profiles are available on a weekly basis from September 1993 to ~~April 2015~~ March 2018 (doi:10.17178/CRYOBSCLIM.CDP.2018.SnowProfile).

Table 3. Overview of the sensors used to gather the hourly and daily snow and soil data, between 1993 and 2017 at Col de Porte, France. Note that outgoing shortwave and longwave radiation is measured using instruments similar to the corresponding incoming radiation, described in Table 2. Note also that snow surface temperature can be derived from the outgoing longwave radiation sensor, in addition to the sensors presented here. The ~~index refers~~ locations refer to ~~the location of the sensor represented in~~ Fig. 2. ~~Text similar to Morin et al. (2012) is underlined.~~

Variable	Location	Sensor	Period of operation	Height	Unit	Time resolution	Integration method
Snow depth	33	BEN ultrasonic depth gauge	... → 1999/2000	3 m	m	hourly	Instantaneous
	33	FNX ultrasonic depth gauge	2000/2001 → 2008/2009	3 m	m	hourly	Instantaneous
	33	Campbell Ultra-sound depth gauge SR50A	2009/2010 → ...	3.5 m	m	hourly	Instantaneous
	32	Dimetix Laser ranger	2010/2011 → ...	3.1 m	m	hourly	Instantaneous
	6[◇]	Campbell Ultra-sound depth gauge SR50	Jan. 2014 → ...	4.1 m	m	hourly	Instantaneous
	6[◇]	Campbell Ultra-sound depth gauge SR50ATH	Jan. 2014 → ...	4.1 m	m	hourly	Instantaneous
	6[◇]	Jenoptik Laser ranger	Jan. 2014 → ...	4.1 m	m	hourly	Instantaneous
	6[◇]	Dimetix Laser ranger	Jan. 2014 → ...	4.1 m	m	hourly	Instantaneous
	hatched	Snowpit (up to three values)	whole record	N.A.	m	≈ weekly	N.A.
Water equivalent of snow cover	16	Cosmic-Ray Neutron sensor	2001/2002 → ...	0 m	kg m^{-2}	daily	24h integration
	16	Cosmic-Ray Neutron sensor[a]	2008/2009 → ...	0 m	kg m^{-2}	daily	24h integration
	hatched	Snowpit (up to three values)	whole record	N.A.	kg m^{-2}	≈ weekly	N.A.
Runoff	11	5 m^2 lysimeter – tipping gauge	... → March 1994	0 m	kg m^{-2} s^{-1}	hourly	Difference
	11	5 m^2 lysimeter – scale	March 1994 → ...	0 m	kg m^{-2} s^{-1}	hourly	Difference
	14	1 m^2 lysimeter – tipping gauge	... → Dec. 1996	0 m	kg m^{-2} s^{-1}	hourly	Difference
	14	1 m^2 lysimeter – scale	Dec. 1996 → ...	0 m	kg m^{-2} s^{-1}	hourly	Difference
Surface temperature	22	Testo term Pyroterm	... → 2016/10	1.2 m[b]	K	hourly	Instantaneous
	21	Campbell IR120	Nov. 2015 → ...	0.8 m[b]	K	hourly	Instantaneous
	28	Heitronics KT15	2010/2011 → ...	3.2 m	K	hourly	Instantaneous
	4[◇]	Campbell IR120	Jan. 2014 → ...	4.1 m	K	hourly	Instantaneous
Soil temperature	24	PT 100/3 wires	... → 1996/1997	−0.1 m	K	hourly	Instantaneous
	24	PT 100/ 4 wires	1997/1998 → ...				
	24	PT 100/ 3 wires	... → 1996/1997	−0.2 m	K	hourly	Instantaneous
	24	PT 100/ 4 wires	1997/1998 → ...				
	24	PT 100/ 3 wires	... → 1996/1997	−0.5 m	K	hourly	Instantaneous
	24	PT 100/ 4 wires	1997/1998 → ...				
	23	PT 100/ 4 wires	Oct. 2012 → ...	−0.05 m	K	hourly	Instantaneous
	23	PT 100/ 4 wires	Oct. 2012 → ...	−0.10 m	K	hourly	Instantaneous
	23	PT 100/ 4 wires	Oct. 2012 → ...	−0.20 m	K	hourly	Instantaneous
	23	PT 100/ 4 wires	Oct. 2012 → ...	−0.30 m	K	hourly	Instantaneous
Soil moisture	23	Delta-T ML2x ThetaProbe Moisture sensor	2012/10 → ...	−0.05 m	m^3 m^{-3}	hourly	Instantaneous
	23	Delta-T ML2x ThetaProbe Moisture sensor	Oct. 2012 → ...	−0.10 m	m^3 m^{-3}	hourly	Instantaneous
	23	Delta-T ML2x ThetaProbe Moisture sensor	Oct. 2012 → ...	−0.20 m	m^3 m^{-3}	hourly	Instantaneous
	23	Delta-T ML2x ThetaProbe Moisture sensor	Oct. 2012 → ...	−0.30 m	m^3 m^{-3}	hourly	Instantaneous
Settling disks temp.	27 and 29	PT 100/3 wires	... → 1996/1997	variable	K	hourly	Instantaneous
	27 and 29	PT 100/ 4 wires	1997/1998 → ...				
Settling disks height	27 and 29	In-house positioning system	whole record[c]	variable	m	hourly	Instantaneous
Ground flux	24	Hukseflux HFP01	since 2010/2011	0	W m^{-2}	hourly	Instantaneous

[a] Sensor including shielding for ground-originating neutrons (reduced data scatter).

[b] Height adjusted manually above snow surface (≈ weekly).

[c] Progressive migration from mercury to solid state electric contact.

[◇] The sensors have been installed for the WMO SPICE project and are used in this study only to complement the dataset if a problem exists for the reference sensor.

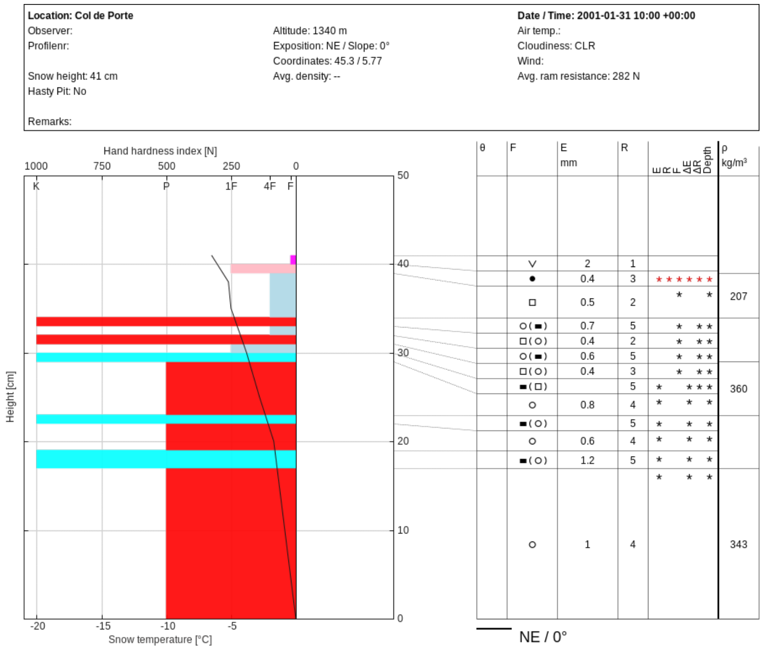

Figure 6. Example of snow profile measured on 13 January 2001 vizualized using niViz software.

2.5 1960-2017 Data

Table 4 describes the daily dataset that combines snow and meteorological measurements. The dataset is provided in netCDF format (doi:10.17178/CRYOBSCLIM.CDP.2018.MetSnowDaily). Variable names correspond to the names listed in ~~Tab.~~ Table 4. Within this daily dataset, the total precipitation dataset is not corrected for undercatch, in contrary to rain and snow datasets (starting in Sept. 1993). The total precipitation dataset is also not measured by the same sensor ~~as~~ used for the rain and snow datasets (cf ~~Tab.~~ Table 4). The total precipitation dataset is measured with the PG2000 sensor~~thus mitigating the impact of the undercatch correction~~, for which the undercatch plays a minor role compared to the GEONOR due to the 10 times larger collecting surface area (Table 2). In addition, the total precipitation time ~~serie~~ series may be qualified as inhomogeneous in time due to the various changes in precipitation gauges. The daily SWE automatic measurements (~~loc. 16~~location 16, Table 3) are discarded for snow season 2015/2016 due to a disfunction of the sensor. Note also that the daily albedo data are uncorrected for local snow surface slope.

The hourly meteorological dataset that contains the whole SAFRAN reanalysis (Durand et al., 2009a) at Col de Porte for the period 1960-2017 is provided in order to drive snowpack simulation over the whole period. The dataset is provided in netCDF format (doi:10.17178/CRYOBSCLIM.CDP.2018.MetSafran) in the standard format for SURFEX meteorological inputs (Vionnet et al., 2012; Masson et al., 2013). The solar mask measured in 1998 (Fig. 3) is accounted for in this dataset.

Table 4. Description of the daily dataset between 1960 and 2017 at Col de Porte, France. The ~~index refers~~ locations refer to ~~the location of the sensor represented in~~ Fig. 2.

Variable	Location	Sensor	Period of operation	Unit	Description
T_{min}	12	PT100	... → 1993	K	Min. temp. between 00:00 (day D) and 24:00 (day D)
	12	cf Table 2	1993 → ...	K	Min. temp between 06:00 (day D-1) and 06:00 (day D)
T_{max}	12	PT100	... → 1993	K	Max. temp. between 00:00 (day D) and 24:00 (day D)
	12	cf Table 2	1993 → ...	K	Max. temp between 06:00 (day D) and 06:00 (day D+1)
snow_depth_auto	close to 33	automatic sensor	... → 1977/1978	m	Snow depth 06:00 (day D)
	33	Ultra-sound depth gauge BEN	1978/1979 → 1999/2000	m	Snow depth 06:00 (day D)
	33-6	cf Table 3	1993 → ...	m	Snow depth 06:00 (day D)
snow_depth_pit	hatched	manual	1963/1964 → 7 Feb. 1996	m	Irregular frequency
	hatched	manual	8 Feb. 1996 → ...	m	Weekly
snow_depth_pit_north	hatched	manual	2001/2002 → ...	m	Weekly
snow_depth_pit_south	hatched	manual	2001/2002 → ...	m	Weekly
swe_auto	16	cf Table 3	2001/2002 → ...	kg m^{-2}	Daily (not available for 2015-2016)
swe_pit	hatched	manual	1963/1964 → 7 Feb. 1996	kg m^{-2}	Irregular frequency, SWE core 38.5 and 25. cm^2
	hatched	manual	8 Feb. 1996 → ...	kg m^{-2}	Weekly, SWE core 100 cm^2
swe_pit_north	hatched	manual	2001/2002 → ...	kg m^{-2}	Weekly, SWE core 100 cm^2
swe_pit_south	hatched	manual	2001/2002 → ...	kg m^{-2}	Weekly, SWE core 100 cm^2
total_precipitation	9	cf Table 2	1960/1961 → 2004/2005	kg m^{-2}	Daily sum of precipitation not corrected for undercatch 06:00 (day D) to 06:00 (day D+1)
rain$^{\diamond}$	20	cf Table 2	1993/1994 → ...	kg m^{-2}	Daily sum of corrected liquid precipitation, 06:00 (day D) to 06:00 (day D+1)
snow$^{\diamond}$	20	cf Table 2	1993/1994 → ...	kg m^{-2}	Daily sum of corrected solid precipitation, 06:00 (day D) to 06:00 (day D+1)
height of new snow	33,27	calculated from snow depth measurement and settlement disks	whole record	cm	Daily sum of new snow, 06:00 (day D) to 06:00 (day D+1)
albedo_daily	26 and 31	cf Table 2	2005/2006 → ...	NA	Ratio of the daily sums of reflected and incident shortwave radiations
albedo_daily_flag	26 and 31	NA	2005/2006 → ...	NA	Number of hourly measurements used to calculate daily albedo

$^{\diamond}$ Note that rain and snow variables are provided only when *in situ* measurements are available (i.e *in situ* flag of ~~Tab.~~ Table 2 - see also ~~figure~~ Fig. 4 in Morin et al., 2012).

3 Spatial variability and measurements uncertainties

The dataset presented in this study is, like any observation dataset, affected by different sources of uncertainties. Regardless of whether these data ~~should be~~ are used for model evaluation or process ~~study~~studies, characterizing their associated uncertainties is essential for ~~a~~ proper use of the data. The uncertainties of the dataset may come from ~~measurements~~ measurement uncertainties (including instrumental and environmental uncertainties) but also from the spatial variability of the variables within the measurement plot.

A lower bound of the uncertainty for each variable can be estimated from the information provided by the sensor manufacturer. Some variables are measured at different locations within the field sites and by different sensors. This provides a better insight of the uncertainty associated ~~to~~ with both sources for each variable. Lafaysse et al. (2017) already provided a first estimate of the ~~uncertainty associated to~~ uncertainties associated with snow depth, ~~snow water equivalent~~ water equivalent of snow cover, bulk density, broadband albedo, soil temperature and snow surface temperature. In this section, we extend the period and the number of points used for the ~~uncertainties evaluation~~ uncertainty evaluations for snow depth, ~~snow water equivalent~~ water equivalent of snow cover and soil temperature for which several measurements are available over a sufficiently long period. We also provide ~~uncertainties assessment~~ uncertainty assessments of the direct/diffuse incident shortwave radiation estimates (cf ~~sec. 2.3.1~~ Sect. 2.3.1 for the calculation of the estimates). Note that an update on the uncertainties for snow surface temperature and broadband albedo is not provided in this study (lack of a sufficient number of sensors) though their uncertainty estimates are crucial for snow model evaluation. In this respect, we recommend the use of uncertainty values provided in Lafaysse et al. (2017) for these two variables.

3.1 Direct/diffuse shortwave incoming radiation

A first source of uncertainties in the calculation of the distribution of the measured broadband shortwave radiation into diffuse and direct radiation originates from the uncertainties of the mask used for the calculation (cf ~~see~~Sect. 2, Fig. 3). Using the methodology explained in ~~See~~Sect. 2.3.1, we estimate the direct and diffuse shortwave incoming radiation based on the mask from 1998 and the mask from 2018 for two snow seasons (~~Sept.~~ 1 ~~st~~ September to 30 June) : 2015-2016 and 2016-2017. The mean difference (mask measured in ~~2017~~ 2018 minus mask measured in 1998) and root mean square deviation (RMSD) computed between diffuse components (over non zero values only) are -1.30 W m^{-2} and 10.1 W m^{-2}. The mean difference and RMSD for the diffuse to total ratio are -0.02 and 0.10, respectively. The histogram of differences ~~are~~ is provided in Fig. 7a.

The accuracy of the methodology described in ~~See~~Sect. 2.3.1 has also been evaluated using the measurements of total and diffuse ~~radiations from location 2~~ radiation from location 5 (at 10 m above ground) and the mask measured in October 2017 at the same location. The comparison is done from ~~September~~ 1 ~~st~~ September 2016 to 30 June 2017 during daylight (i.e., if total measured shortwave is larger than 4 W m^{-2}). The mean difference between the estimated and simulated diffuse component is -15.26 W m^{-2} (RMSD: 53 W m^{-2}). The mean difference and RMSD computed for the diffuse to total ratio are -0.08 and 0.21~~. The histograms of differences are~~ , respectively. The histogram of differences is provided in Fig. 7b. This shows that the

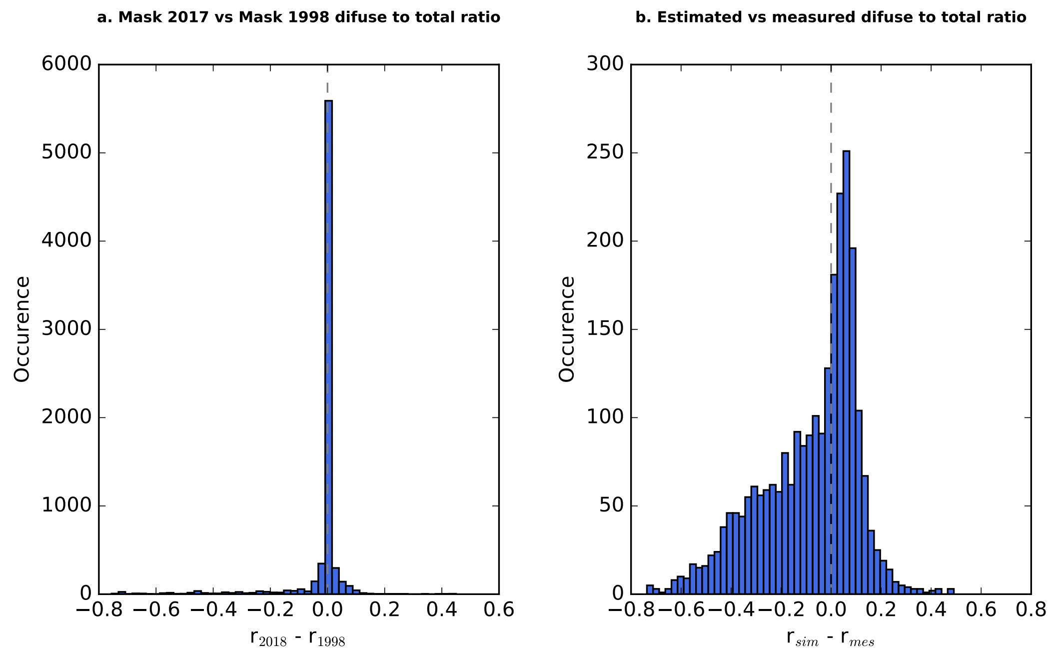

Figure 7. Comparison of different broadband diffuse to total shortwave radiation ratio, r. (a) Difference in ratio estimated with the mask measured in June 2018 and in June 1998 at ~~location 25.~~ location 25. Statistics are calculated during daylight from ~~Sep.~~ 1 ~~st~~ September 2015 to 30 June 2017 excluding July and August for each year. (b) Difference in ratio estimated with the 2017 mask (measured at ~~location 5~~location 5, 21 October ~~21st~~ 2017) and the measured ratio at ~~location 5.~~ location 5. Statistics are calculated during daylight from ~~September~~ 1 ~~st~~ September 2016 to 30 June 2017.

estimation of the diffuse radiation ~~is slightly biased low~~ has a slightly negative bias and that this uncertainty has to be taken into account for applications such as radiative balance calculation for which the direct/diffuse distribution has a significant impact. It also shows that the methodology applied to partition the direct and diffuse components has a larger impact on the uncertainty than the change in solar masks shown in Fig. 3.

3.2 Snow depth

Table 5. Statistics of the comparisons between the different snow depth measurements represented in Fig. 8.

Sensors	Number of times	Deviation (m)	RMSD (m)	Period
Nivose 1 - h_{ref}	22498	-0.007	0.039	Sept. 2009 to June 2016
Mast - h_{ref}	22225	0.013	0.036	Sept. 2009 to June 2016
Pit - h_{ref}	874	0.053	0.077	Sept. 1960- June 2017
North Pit - h_{ref}	261	0.124	0.128	Sept. 2001 to June 2017
South Pit - h_{ref}	261	0.107	0.108	Sept. 2001 to June 2017

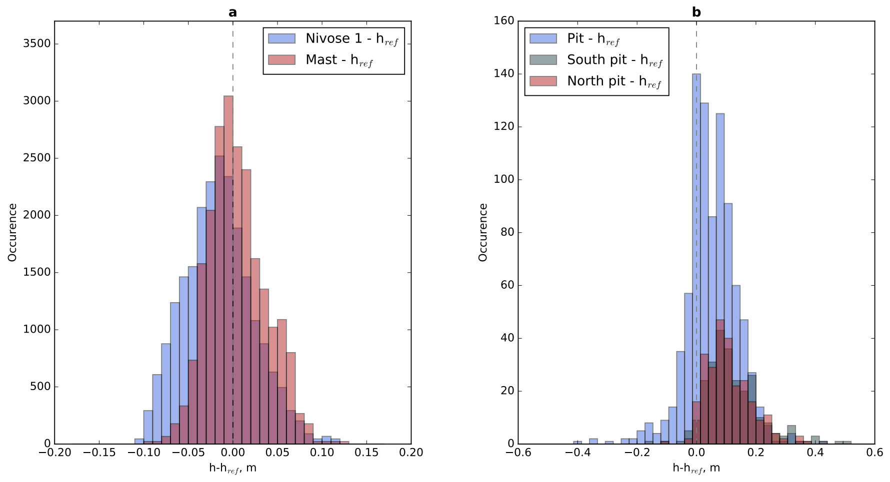

Figure 8. Comparison of snow depth measurements at different locations. h_{ref} corresponds to ~~location 33.~~ location 33. (a) Difference in measured snow depth between the ultrasound sensor placed ~~on~~ at the Nivose 1 ~~location (Fig. 2)~~ location and the reference snow depth (~~locations 32-33 in Fig. 2~~locations 32-33) in blue. In red, differences between the measured snow depth at ~~location 6 (Fig. 2)~~ location 6 and the reference snow depth. The ~~difference~~ differences are calculated from snow season 2009/2010 to snow season 2015/2016 using only data from 20 ~~Sept.~~ September to 10 June. Data where both locations indicate 0 snow depth are excluded from the statistics. (b) Difference in measured snow depth between the manual snow depth measurements at ~~snowpit field location (Fig. 2)~~ snowpit field location and reference automatic snow depth (~~location 33~~location 33) in blue, between manual snow depth measurement in the snow pit south field and reference in grey and snow pit north field and reference in red. Difference values are calculated over the 1960-2017 period for the pit value and 2001-2017 for north and south pits. Data where both locations indicate 0 snow depth are excluded from the statistics. Corresponding statistics are provided in ~~Tab.~~ Table 5.

Figure 8 compares the snow depth reference value mostly measured at ~~location 32-33~~location 32-33, h_{ref} ~~(Fig. 2)~~ with several other measurements of snow depth : in panel (a) with respect to automatic snowdepth measurements at ~~locations "Nivose 1" and 6 (see Fig. 2) and~~ locations "Nivose 1" and 6 and in panel (b) with respect to manual snow depth measurement in snow pit fields (main, north and south, blue hatched areas in Fig. 2). For panel (a), the comparison is done over the 2009-2016 period and ~~the automated measurement have been manually corrected for any blank period and measurements inconsistency.~~ any blank or inconsistent measurement period in the "Nivose 1" (resp. mast) sensor was discarded from the comparison. For panel (b), the comparison with the main snow pit field is done over 1960-2017 and for the ~~pits~~ south and north pits over 2001-2017. For each sensor, the number of points used to calculate the statistics are in ~~Tab.~~ Table 5.

Figure 8a and Table 5 show that the three automatic measurements exhibit deviations lower than 1.3 cm and that the RMSD is lower than 4 cm. Higher discrepancies are found between the reference automatic measurements and the manual measurements (~~Figure~~ Fig. 8b) with mean deviation reaching almost ~~14~~ 13 cm and RMSD ~~14~~ 13 cm. These higher difference values might be attributed to the local slope, aspect, and small topographic features within the three snow pit ~~fields area~~ field areas and to the higher ~~measurements uncertainties associated to~~ measurement uncertainty associated with manual measurements. Extreme difference values corresponds to the end of the snow season when the snow cover is patchy. Picard et al. (2016) installed during the 2014-2015 snow season an automatic scanning laser meter close to ~~location 6~~ location 6 that scanned an area of 100-200 m^2. During this snow season, the laser measurements indicated a spatial varibility of the snow depth within the footprint that can reach 7-10 cm (RMSD). We thus recommend the use of $\pm$ 10 cm uncertainty value for snow depth in any evaluation to represent the spatial variability within the site, ~~that is~~ comparable to the values used in Lafaysse et al. (2017).

3.3 ~~Snow water~~ Water equivalent of snow cover

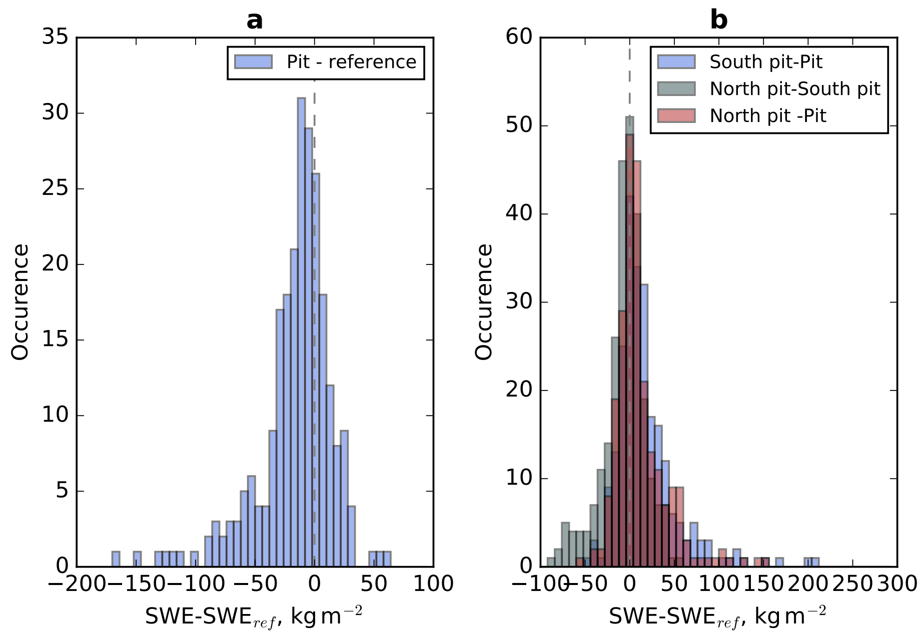

Figure 9. Comparison of SWE measurements at different locations. (a) Difference in measured SWE between the manual measurement in the snow pit field (Fig. 2) and the reference automatic SWE (SWE$_{\mathrm{ref}}$, ~~location 16~~ location 16 in ~~Fig. 2) in~~ blue. The difference are calculated over the period 2001-2017 (no reference data for 2015/2016 snow season). Data where both locations indicate 0 SWE are excluded from the statistics. Note that the manual measurements from snow pit south and north are used for the SWE sensor (~~location 16~~location 16) calibration. (b) Difference in manually measured SWE between the snowpit field south and the snow pit field location in blue, between the snow pit field north and south locations in green and snow pit north field and snow pit field in red. Difference are calculated over the 2001-2017 period. Data where both locations indicate 0 SWE are excluded from the statistics. Numerical values are provided in ~~Tab.~~ Table 6.

Figure 9 and ~~Tab. 6 compares~~ Table 6 compare the SWE automatic measurements at ~~location 16 (Fig. 2)~~ location 16 with the manual ~~measured in~~ measurements from the main snow pit field (panel a) and the three locations for manual SWE measurements (panel b). The statistics are calculated over the ~~2001-2016~~ 2001-2017 period. It must be underlined that the ~~SWE~~

Table 6. Statistics of the comparisons between the different SWE measurements represented in Fig. 9.

Sensors	Number of dates	Deviation (kg m^{-2})	RMSD (kg m^{-2})	Period
Pit - SWE_{ref}	244	-16.83	24.44	Sept. 2001 to June 2017
South Pit - Pit	239	17.37	25.09	Sept. 2001 to June 2017
North Pit - South Pit	260	-6.69	17.66	Sept. 2001 to June 2017
South Pit - Pit	239	11.84	20.01	Sept. 2001 to June 2017

~~automatic~~ automatic SWE sensor is calibrated using the manual measurements at snow pit fields south and north. The average of the annual maximum value of SWE_{ref} during this period is 389 $\pm$ 104 kg m^{-2} .

Figure 9 and ~~Tab.~~ Table 6 show that the mean difference between the automatic and ~~the~~ manual measurements in the main snow pit field reaches -17 kg m^{-2} with RMSD of almost 25 kg m^{-2}. The comparison between the three locations of manual measurements displays RMSD reaching 25 kg m^{-2}~~.~~, i.e. 8.6 % of average peak SWE values. This value is consistent with the spatial variability of snow depth and can probably be used as an estimate of the uncertainty associated ~~to~~ with the SWE dataset both due to ~~measurements~~ measurement errors and spatial variability.

3.4 Soil temperature

Table 7. Statistics of the comparisons between the different soil temperature measurements represented in Fig. 10.

Sensors	Depth (cm)	Number of dates	Deviation (K)	RMSD (K)	Period
s2_loc23_10 - s1_loc23_10	10	15084	0.034	0.110	Dec. 2015 to June 2017
s3_loc23_10 - s1_loc23_10	10	15084	-0.094	0.244	Dec. 2015 to June 2017
s3_loc23_10 - s2_loc23_10	10	15084	0.128	0.182	Dec. 2015 to June 2017
loc_23 - loc_24	10	11396	-0.108	0.415	Dec. 2015 to June 2017 (snow season)
loc_23 - loc_24	10	3688	-1.059	1.100	Dec. 2015 to June 2017 (summer)
s2_loc23_20 - s1_loc23_20	20	15084	0.093	0.118	Dec. 2015 to June 2017
loc_23 - loc_24	20	11396	-0.224	0.390	Dec. 2015 to June 2017 (snow season)
loc_23 - loc_24	20	3688	-0.943	0.961	Dec. 2015 to June 2017 (summer)

Figure 10 and ~~Tab.~~ Table 7 compare the different soil temperature measurements at 10 and 20 cm depths for ~~locations 23 and 24 (Fig. 2). The first column~~ locations 23 and 24. The left panels in Fig. 10 display the statistics of the different temperature probes ~~located index 23 and spaces~~ at location 23 and spaced by roughly 10 cm ~~.~~ (s1_loc23_10, s2_loc23_10 and s3_loc23_10 and s1_loc23_20, s2_loc23_20, resp.). It indicates that the RMSD between the 3 probes is lower than 0.25 K ~~. The second column compares location 24~~ (Table 7). The right panels in Fig. 10 compare locations 24 (old sensors) and 23 (new sensors mean) for two periods : summer (20 June to 10 October) and snow season (11 October to 19 June). During the snow season, the two locations show a small mean deviation of -0.11K and an RMSD of 0.42 K, while during summer the mean deviation is roughly -1.06 K leading to RMSD of 1.10 K (Table 7). Note that these two locations are spaced by only a few meters ~~only~~ (see Fig. 2). The temperature difference between the two sensors may be attributed to differences in soil properties, local topography

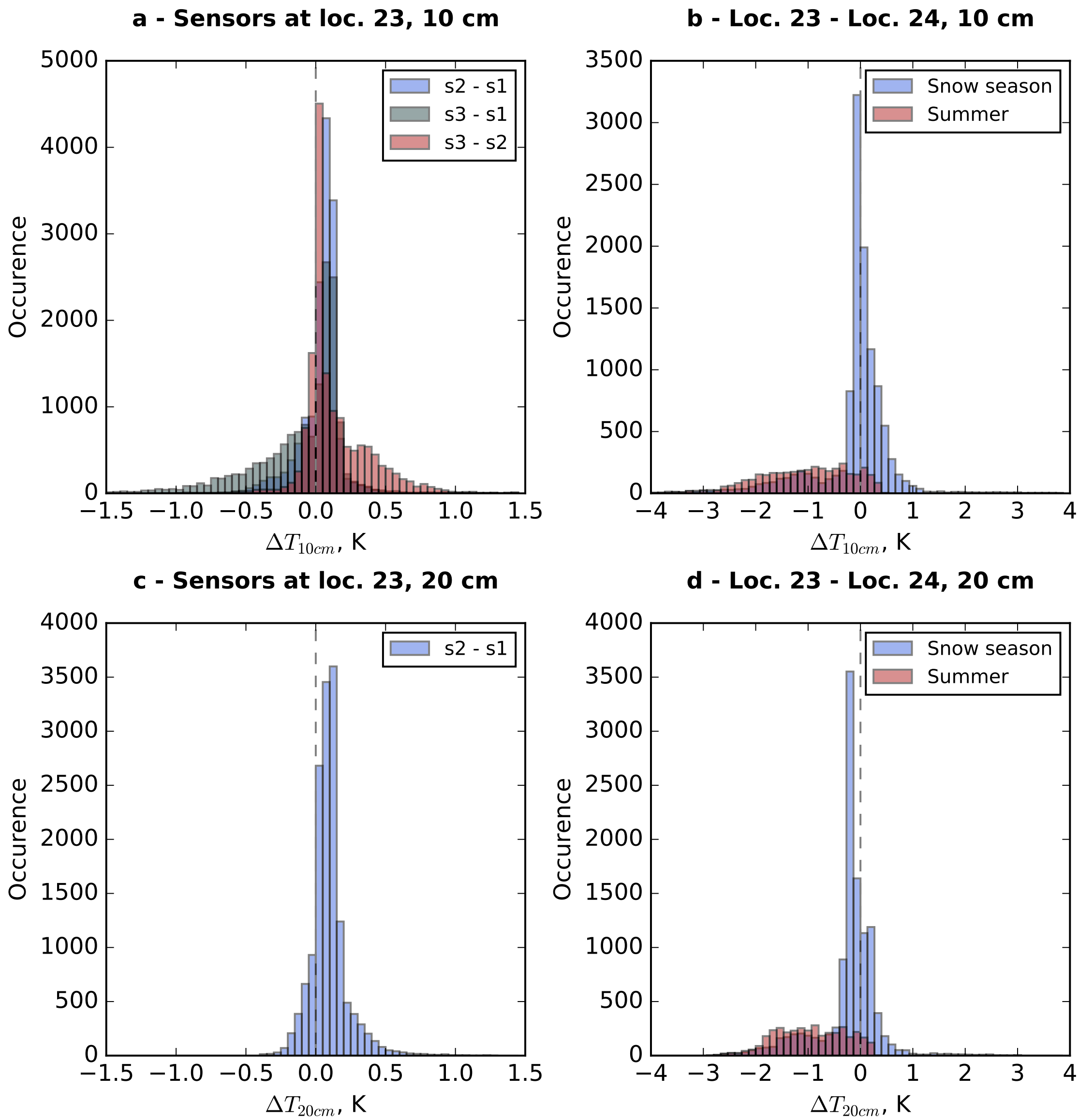

Figure 10. Comparison between the different soil temperature measurements at 10 cm (panels a and b) and 20 cm (panels c and d) depths. Panels a and c compare the new sensors (3 probes~~roughly 10 cm away of each other~~) at ~~location 23~~ location 23 at -10 cm and 2 probes ~~roughly 10 cm away of each other~~ at -20 cm). Panels b and ~~c compares~~ d compare the average values of the new sensors (~~location 23~~location 23) to the old ones (~~location 24~~location 24). Statistics are calculated from December 2015 to July 2017. Summer (panels b and d, in red) corresponds to the period between 20 June 2016 and 10 October 2016 and 20 June 2017 to 31 July 2017. The rest of the dates corresponds to snow season (panels b and d, in blue). Numerical values are provided in ~~Tab.~~ Table 7.

and shading. The larger differences in summer may be due to (i) larger heterogeneity in soil wetness and (ii) the absence of the snow cover that spatially tempers the surface temperature signal in winter.

From these observations, a lower bound of the uncertainty of the soil temperature measurements (spatial variability and measurements errors) is roughly 1.10 K during summer, roughly 0.42 K during the snow season and a little higher than 0.5 K averaged over the whole year.

4 Data use

4.1 Temperature, snow depth and precipitation since 1960

Fig. 11 displays the evolution of mean snow depth, air temperature and total precipitation from ~~Dec.~~ 1 ~~st to April~~ December to 30 ~~th~~ April of each snow season for the whole period of the dataset (Dec. 1960 - April 2017). This figure shows an example of a direct use of the dataset to study the past evolution of winter conditions at Col de Porte. It demonstrates that the decrease in mean snow depth ~~reduction~~ between 1960-1990 and 1990-2017 is 39 cm (40 % of the mean snow depth for 1960-1990), while the air temperature has increased ~~of~~ by 0.90 °C over the same period ~~and~~ while the total precipitation does not exhibit a significant trend. This indicates that at this site, the reduction of the snow cover is mainly due to the increase in temperature and its consequences (e.g. higher snow/rain limit ~~when~~ during precipitation and higer melt rates). ~~This long time serie contributes~~ These long time series contribute to placing long term climate change impact studies on mountain snow conditions in the context of past changes (Verfaillie et al., 2018).

4.2 Snow model evaluation

This dataset has been widely used to drive and evaluate snow models (e.g. ~~Essery et al., 2013; Magnusson et al., 2015; Decharme et al., 2016; Lafaysse et al., 2017; Piazzi et al., 2018~~Essery et al., 2013; Wever et a A list of the studies using CDP dataset is available at http://www.umr-cnrm.fr/spip.php?article533. ~~It has also been included in the Earth System Model - Snow Model Intercomparison Project ().~~

5 Data availability

The database (doi:10.17178/CRYOBSCLIM.CDP.2018) presented and described in this article is available for download at http://dx.doi.org/10.17178/CRYOBSCLIM.CDP.2018. ~~Tab.~~ Table 8 provides the links to the different datasets.

6 Conclusions

This paper describes and provides access to the daily snow and meteorological dataset measured at the Col de Porte site, 1325 m a.s.l, Chartreuse, France for the period 1960-2017. The hourly dataset of snow and meteorological observations for the period 1993-2017 is made available along with weekly snow profiles from September 1993 to March 2018, soil properties and

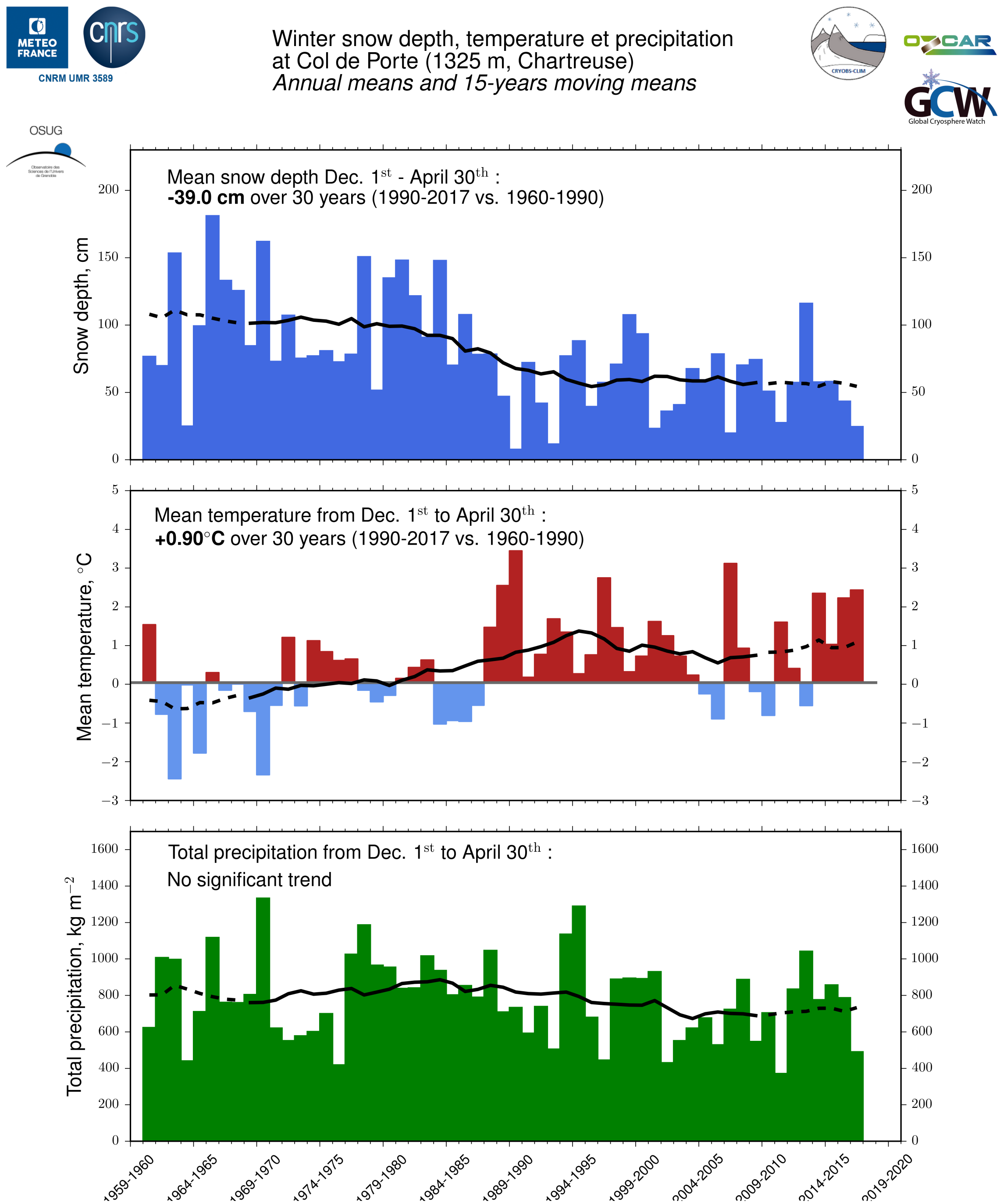

Figure 11. Evolution of mean snow depth, air temperature and total precipitation over 1960-2017. The mean and total values are calculated over the period ~~Dec.~~ 1 ~~st~~ December to ~~April~~ 30 ~~th~~ April of each snow season. The black lines are ~~the 15 years~~ 15-year moving means.

Table 8. Link to the dataset repository

Dataset	Period	Format	Repository
Solar Mask	July 1998 and June 2018	csv	http://dx.doi.org/10.17178/CRYOBSCLIM.CDP.2018.SolarMask
Soil properties	29 September 2008 and October 2nd 2012	csv	http://dx.doi.org/10.17178/CRYOBSCLIM.CDP.2018.Soil
Hourly in situ meteorological data	August 1st 1993 to 31 July 2017	netCDF	http://dx.doi.org/10.17178/CRYOBSCLIM.CDP.2018.MetInsitu
Hourly SAFRAN meteorological data	August 1st 1960 to 31 July 2017	netCDF	http://dx.doi.org/10.17178/CRYOBSCLIM.CDP.2018.MetSafran
Daily snow and meteorological data	August 1st 1960 to 31 July 2017	netCDF	http://dx.doi.org/10.17178/CRYOBSCLIM.CDP.2018.MetSnowDaily
Hourly snow data	August 1st 1960 to 31 July 2017	netCDF	http://dx.doi.org/10.17178/CRYOBSCLIM.CDP.2018.HourlySnow
Snow profiles	September 1993 to March 2018	caaml	http://dx.doi.org/10.17178/CRYOBSCLIM.CDP.2018.SnowProfile

solar radiation masks. Based on measurements at several locations within the measurement field, we estimated the uncertainties and spatial variability of : the ratio between solar diffuse and total irradiance, snow depth, water equivalent of snow cover and soil temperature. The data are placed on the repository of the Observatoire des Sciences de l'Univers de Grenoble (OSUG) datacenter : http://dx.doi.org/10.17178/CRYOBSCLIM.CDP.2018.

Author contributions. Y.L. and J.-M. P. endorse the responsability of the experimental site and of the instruments. M.D. led the consolidation of the data set and wrote this manuscript together with all co-authors. E. L. and J.-M. P. ensure the proper working of the instruments.

Acknowledgements. Many thanks are expressed to people of CNRM/CEN who have assisted in the collection, collation and archive of this unique dataset. We thank in particular É. Pougatch, Y. Danielou, J.-L. Dumas for their crucial work on the database. Generating and distributing this dataset directly benefitted from the LabEX OSUG@2020 (ANR10 LABX56). The authors are also thankful to EDF/DTG, ONF, SOERE CryObsClim, GCW and the IDEX Univ. Grenoble Alpes Cross Disciplinary Project Trajectories. The authors also ~~thanks~~ thank Arnaud Foulquier (LECA) for his help with soil and vegetation properties measurements and Laurent Bourges (OSUG) for the establishment of the data repository and the allocation of dedicated dois. The authors are grateful to R. Essery, C. Fierz and one anonymous referee for their useful comments on the manuscript, and to M. Bavay and C. Fierz for their help with niViz and caaml formats.

References

Berliand, M.: Determining the net long-wave radiation of the Earth with consideration of the effect of cloudiness, Izv. Akad. Nauk. SSSR Ser. Geofiz, 1, 64–78, 1952.

Bouilloud, L. and Martin, E.: A coupled model to simulate snow behavior on roads, J. Appl. Meteorol., 45, 500–516, 2006.

Brun, E., David, P., Sudul, M., and Brunot, G.: A numerical model to simulate snow-cover stratigraphy for operational avalanche forecasting, J. Glaciol., 38, 13 – 22, http://refhub.elsevier.com/S0165-232X(14)00138-4/rf0155, 1992.

Decharme, B., Martin, E., and Faroux, S.: Reconciling soil thermal and hydrological lower boundary conditions in land surface models, Journal of Geophysical, 118, 7819–7834, doi:10.1002/jgrd.50631, 2013.

Decharme, B., Brun, E., Boone, A., Delire, C., Le Moigne, P., and Morin, S.: Impacts of snow and organic soils parameterization on northern Eurasian soil temperature profiles simulated by the ISBA land surface model, The Cryosphere, 10, 853–877, doi:10.5194/tc-10-853-2016, http://www.the-cryosphere.net/10/853/2016/, 2016.

Dumont, M., Arnaud, L., Picard, G., Libois, Q., Lejeune, Y., Nabat, P., Voisin, D., and Morin, S.: In situ continuous visible and near-infrared spectroscopy of an alpine snowpack, The Cryosphere, 11, 1091–1110, doi:10.5194/tc-11-1091-2017, https://www.the-cryosphere.net/11/1091/2017/, 2017.

Durand, Y., Giraud, G., Brun, E., Mérindol, L., and Martin, E.: A computer-based system simulating snowpack structures as a tool for regional avalanche forecasting, J. Glaciol., 45, 469–484, 1999.

Durand, Y., Giraud, G., Laternser, M., Etchevers, P., Mérindol, L., and Lesaffre, B.: Reanalysis of 47 Years of Climate in the French Alps (1958–2005): Climatology and Trends for Snow Cover, J. Appl. Meteor. Climat., 48, 2487–2512, doi:10.1175/2009JAMC1810.1, 2009a.

Durand, Y., Giraud, G., Laternser, M., Etchevers, P., Mérindol, L., and Lesaffre, B.: Reanalysis of 44 Yr of Climate in the French Alps (1958–2002): Methodology, Model Validation, Climatology, and Trends for Air Temperature and Precipitation., J. Appl. Meteor. Climat., 48, 429–449, doi:10.1175/2008JAMC1808.1, 2009b.

Essery, R., Morin, S., Lejeune, Y., and Menard, C. B.: A comparison of 1701 snow models using observations from an alpine site, Advances in water resources, 55, 131–148, doi:10.1016/j.advwatres.2012.07.013, 2013.

Essery, R., Kontu, A., Lemmetyinen, J., Dumont, M., and Ménard, C. B.: A 7-year dataset for driving and evaluating snow models at an Arctic site (Sodankylä, Finland), Geoscientific Instrumentation, Methods and Data Systems, 5, 219–227, doi:10.5194/gi-5-219-2016, http://www.geosci-instrum-method-data-syst.net/5/219/2016/, 2016.

Etchevers, P.: Modélisation de la phase continentale du cycle de l'eau à l'échelle régionale. Impact de la modélisation de la neige sur l'hydrologie du Rhône, Ph.D. thesis, PhD thesis, Université Paul Sabatier, Toulouse, 2000.

Etchevers, P., Martin, E., Brown, R., Fierz, C., Lejeune, Y., Bazile, E., Boone, A., Dai, Y.-J., Essery, R., Fernandez, A., Gusev, Y., Jordan, R., Koren, V., Kowalczyk, E., Nasonova, N. O., Pyles, R. D., Schlosser, A., Shmakin, A. B., Smirnova, T. G., Strasser, U., Verseghy, D., Yamazaki, T., and Yang, Z.-L.: Intercomparison of the surface energy budget simulated by several snow models (SNOWMIP project), Ann. Glaciol., 38, 150 – 158, doi:10.3189/172756404781814825, 2004.

Fierz, C., Armstrong, R. L., Durand, Y., Etchevers, P., Greene, E., McClung, D. M., Nishimura, K., Satyawali, P. K., and Sokratov, S. A.: The international classification for seasonal snow on the ground, IHP-VII Technical Documents in Hydrology n 83, IACS Contribution n 1, http://unesdoc.unesco.org/images/0018/001864/186462e.pdf, 2009.

Gaillardet, J., Braud, I., Hankard, F., et al.: OZCAR, the French network of critical zones observatories, Vadoze Zone Journal, in review.

Krinner, G., Derksen, C., Essery, R., Flanner, M., Hagemann, S., Clark, M., Hall, A., Rott, H., Brutel-Vuilmet, C., Kim, H., Ménard, C. B., Mudryk, L., Thackeray, C., Wang, L., Arduini, G., Balsamo, G., Bartlett, P., Boike, J., Boone, A., Chéruy, F., Colin, J., Cuntz, M., Dai, Y., Decharme, B., Derry, J., Ducharne, A., Dutra, E., Fang, X., Fierz, C., Ghattas, J., Gusev, Y., Haverd, V., Kontu, A., Lafaysse, M., Law, R., Lawrence, D., Li, W., Marke, T., Marks, D., Nasonova, O., Nitta, T., Niwano, M., Pomeroy, J., Raleigh, M. S., Schaedler, G., Semenov, V., Smirnova, T., Stacke, T., Strasser, U., Svenson, S., Turkov, D., Wang, T., Wever, N., Yuan, H., and Zhou, W.: ESM-SnowMIP: Assessing models and quantifying snow-related climate feedbacks, Geoscientific Model Development Discussions, 2018, 1–32, doi:10.5194/gmd-2018-153, https://www.geosci-model-dev-discuss.net/gmd-2018-153/, 2018.

Lafaysse, M., Cluzet, B., Dumont, M., Lejeune, Y., Vionnet, V., and Morin, S.: A multiphysical ensemble system of numerical snow modelling, The Cryosphere, 11, 1173–1198, doi:10.5194/tc-11-1173-2017, http://www.the-cryosphere-discuss.net/tc-2016-287/, 2017.

Magnusson, J., Wever, N., Essery, R., Helbig, N., Winstral, A., and Jonas, T.: Evaluating snow models with varying process representations for hydrological applications, Water Resources Research, 51, 2707–2723, 2015.

Masson, V., Le Moigne, P., Martin, E., Faroux, S., Alias, A., Alkama, R., Belamari, S., Barbu, A., Boone, A., Bouyssel, F., Brousseau, P., Brun, E., Calvet, J.-C., Carrer, D., Decharme, B., Delire, C., Donier, S., Essaouini, K., Gibelin, A.-L., Giordani, H., Habets, F., Jidane, M., Kerdraon, G., Kourzeneva, E., Lafaysse, M., Lafont, S., Lebeaupin Brossier, C., Lemonsu, A., Mahfouf, J.-F., Marguinaud, P., Mokhtari, M., Morin, S., Pigeon, G., Salgado, R., Seity, Y., Taillefer, F., Tanguy, G., Tulet, P., Vincendon, B., Vionnet, V., and Voldoire, A.: The SURFEXv7.2 land and ocean surface platform for coupled or offline simulation of Earth surface variables and fluxes, Geoscientific Model Development, 6, 929–960, doi:10.5194/gmd-6-929-2013, 2013.

Morin, S., Lejeune, Y., Lesaffre, B., Panel, J.-M., Poncet, D., David, P., and Sudul, M.: A 18-years long (1993 - 2011) snow and meteorological dataset from a mid-altitude mountain site (Col de Porte, France, 1325 m alt.) for driving and evaluating snowpack models, Earth Syst. Sci. Data, 4, 13–21, doi:10.5194/essd-4-13-2012, 2012.

Piazzi, G., Thirel, G., Campo, L., and Gabellani, S.: A particle filter scheme for multivariate data assimilation into a point-scale snowpack model in an Alpine environment, The Cryosphere, 12, 2287–2306, doi:10.5194/tc-12-2287-2018, https://www.the-cryosphere.net/12/2287/2018/, 2018.

Picard, G., Arnaud, L., Panel, J.-M., and Morin, S.: Design of a scanning laser meter for monitoring the spatio-temporal evolution of snow depth and its application in the Alps and in Antarctica, The Cryosphere, 10, 1495–1511, doi:10.5194/tc-10-1495-2016, https://www.the-cryosphere.net/10/1495/2016/, 2016.

Quéno, L., Karbou, F., Vionnet, V., and Dombrowski-Etchevers, I.: Satellite products of incoming solar and longwave radiations used for snowpack modelling in mountainous terrain, Hydrology and Earth System Sciences Discussions, 2017, 1–33, doi:10.5194/hess-2017-563, https://www.hydrol-earth-syst-sci-discuss.net/hess-2017-563/, 2017.

Raleigh, M., Lundquist, J., and Clark, M.: Exploring the impact of forcing error characteristics on physically based snow simulations within a global sensitivity analysis framework, Hydrology and Earth System Sciences, 19, 3153–3179, 2015.

Sauter, T. and Obleitner, F.: Assessing the uncertainty of glacier mass-balance simulations in the European Arctic based on variance decomposition, Geoscientific Model Development, 8, 3911–3928, doi:10.5194/gmd-8-3911-2015, https://www.geosci-model-dev.net/8/3911/2015/, 2015.

Sicart, J. E., Ramseyer, V., Lejeune, Y., Essery, R., Webster, C., and Rutter, N.: Spatial and Temporal Variabilities of Solar and Longwave Radiation Fluxes below a Coniferous Forest in the French Alps, in: AGU Fall Meeting Abstracts, 2017.

Tuzet, F., Dumont, M., Lafaysse, M., Picard, G., Arnaud, L., Voisin, D., Lejeune, Y., Charrois, L., Nabat, P., and Morin, S.: A multilayer physically based snowpack model simulating direct and indirect radiative impacts of light-absorbing impurities in snow, The Cryosphere, 11, 2633–2653, doi:10.5194/tc-11-2633-2017, https://www.the-cryosphere.net/11/2633/2017/, 2017.

Vauge, P. d. B.: Le gisement solaire-Evaluation de la ressource énergétique, Ciel et Terre, 99, 62, 1983.

Verfaillie, D., Lafaysse, M., Déqué, M., Eckert, N., Lejeune, Y., and Morin, S.: Multi-component ensembles of future meteorological and natural snow conditions for 1500 m altitude in the Chartreuse mountain range, Northern French Alps, The Cryosphere, 12, 1249–1271, doi:10.5194/tc-12-1249-2018, https://www.the-cryosphere.net/12/1249/2018/, 2018.

Vionnet, V., Brun, E., Morin, S., Boone, A., Martin, E., Faroux, S., Moigne, P. L., and Willemet, J.-M.: The detailed snowpack scheme Crocus and its implementation in SURFEX v7.2, Geosci. Model. Dev., 5, 773–791, doi:10.5194/gmd-5-773-2012, 2012.

Wever, N., Fierz, C., Mitterer, C., Hirashima, H., and Lehning, M.: Solving Richards Equation for snow improves snowpack meltwater runoff estimations in detailed multi-layer snowpack model, The Cryosphere, 8, 257–274, doi:10.5194/tc-8-257-2014, 2014.

Williams, C., McNamara, J., and Chandler, D.: Controls on the temporal and spatial variability of soil moisture in a mountainous landscape: the signature of snow and complex terrain, Hydrology and Earth System Sciences, 13, 1325–1336, 2009.